J. Fluid Mech. (2001), *vol.* 449, *pp.* 85–114.
DOI: 10.1017/S0022112001006127 Printed in the United Kingdom

The onset of meandering in a barotropic jet

By N. J. BALMFORTH AND C. PICCOLO

Department of Applied Mathematics and Statistics, School of Engineering,
University of California at Santa Cruz, CA 95064, USA

(Received 10 October 2000 and in revised form 14 May 2001)

This study explores the dynamics of an unstable jet of two-dimensional, incompressible fluid on the beta-plane. In the inviscid limit, standard weakly nonlinear theory fails to give a low-order description of this problem, partly because the simple shape of the unstable normal mode is insufficient to capture the structure of the forming pattern. That pattern takes the form of 'cat's eyes' in the vorticity distribution which develop inside the modal critical layers (slender regions to either side of the jet's axis surrounding the levels where the modal wave speed matches the mean flow). Asymptotic expansions furnish a reduced model which is a version of what is known as the single-wave model in plasma physics. The reduced model predicts that the amplitude of the unstable mode saturates at a relatively low level and is not steady. Rather, the amplitude evolves aperiodically about the saturation level, a result with implications for Lagrangian transport theories. The aperiodic amplitude 'bounces' are intimately connected with sporadic deformations of the vortices within the cat's eyes. The theory is compared with numerical simulations of the original governing equations. Slightly asymmetrical jets are also studied. In this case the neutral modes along the stability boundary become singular; an extension of the weakly nonlinear theory is presented for these modes.

1. Introduction

The dynamics of two-dimensional jets plays an important role in many geophysical and astrophysical flows, ranging from the meander of the Earth's gulf stream to the formation of vortical structures in Jupiter's atmosphere. Two-dimensional jets have also been explored in the laboratory, especially in experiments involving flows in circular or annular geometry (Dolzhanskii, Krymov & Manin 1991; Solomon, Holloway & Swinney 1993; Früh & Read 1999; van de Konijnenberg *et al.* 1999). Key points of interest are how vortices are generated through intrinsic instability, and how mixing proceeds in the unsteady fluid motions that result.

In the present work, we explore meanders of jets in two-dimensional, incompressible fluids on the beta-plane. We focus upon conditions in the vicinity of the onset of instability and in the inviscid limit. These restrictions allow us to investigate analytically the details of the pattern formation problem, and to complement the laboratory experiments and related numerical simulations (Flierl, Malanotte-Rizzoli & Zabusky 1987; Kwon & Mak 1988; van de Konijnenberg *et al.* 1999) which operate in the more strongly viscous and unstable regimes. However, we emphasize that we are mainly concerned with the mathematical details of the weakly viscous problem, rather than the issues raised by laboratory and numerical experiments.

To delineate the problem further, we consider the Bickley jet (with a $\mathrm{sech}^2 y$ velocity profile); the stability boundaries of this flow are partly known analytically and it is

a popular model of a wake and in the experiments with rotating annuli. Our goal is a weakly nonlinear theory for the meanders of the jet. However, this theory cannot be derived as straightforwardly as in other pattern formation problems because we operate close to the inviscid limit. In such conditions, theory of linear shear flow dynamics is plagued by singularities that occur along lines for which the mean flow matches the speed of a neutral wave; these are usually termed 'critical level' singularities in fluid mechanics. For jets, there are two such levels, lying to either side of the jet axis.

Despite this problematic feature of linear theory, the instability of the flow is described by a smooth discrete eigenmode which has no critical-level singularities. Thus the stability properties of the flow can be detected by conventional normal-mode techniques. Unfortunately, one cannot continue to ignore critical-level problems when one advances to the weakly nonlinear analysis of the unstable modes close to onset.† This theory fails completely because critical-level singularities enter at all higher orders of the asymptotic expansion and become progressively worse as one proceeds along the asymptotic sequence. The divergences signify the breakdown of the conventional solution in slender regions surrounding the singular levels. Inside these 'critical layers', a different solution is needed; specifically, one that varies on a much finer spatial scale. Physically, what happens is that the evolving unstable disturbance generates a pattern with sharp gradients in the critical layers. This structure is not captured by the simple geometry of the unstable eigenmode, and takes the form of a chain of vortices (a cat's eye pattern). Thus, to counter the breakdown of the regular expansion, one finds 'inner' solutions inside the critical layers and matches these to the usual weakly nonlinear solution, which remains valid outside the critical layers (the 'outer region'). In other words, we exploit a matched asymptotic expansion.

The asymptotic analysis follows a similar route to that taken for unstable shear layers (Churilov & Shukhman 1987; Goldstein & Leib 1988; Goldstein & Hultgren 1998), compressible shear instability (Balmforth 1999), disturbed vortices (Balmforth, Llewellyn Smith & Young 2000) and electrostatic plasma instability (del Castillo-Negrete 1998). These other examples are all characterized by equilibrium states for which the profile of the background fluid motion is monotonic, and consequently, there is only a single critical layer. By contrast, for jet profiles, the modes have two critical levels, suggesting a richer behaviour. As we find for the particular problem considered here, however, there is no essential difference for profiles such as the Bickley jet which are symmetrical under reflection about the jet axis; the outcome of the asymptotic analysis is the same as for the monotonic cases.‡ This highlights a key fact about the particular bifurcation to instability that we explore: the asymptotic analysis furnishes a reduced model of a 'universal' form. In fact, the system is a version of the 'single-wave model' used in plasma physics (O'Neil, Winfrey & Malmberg 1971; Tennyson, Meiss & Morrison 1994). One of our main aims here is to give the first systematic exploration of this universal system.

† From the mathematical perspective, the singularities in the linear eigenvalue problem reflect a continuous spectrum of singular, neutral modes with critical levels; at onset, the unstable mode is embedded within this continuous spectrum, which is why centre-manifold theory fails in this instance.

‡ Leib & Goldstein (1989) have also explored the Bickley jet, focusing on a different, modal interaction problem. Their analysis explores dynamics that is indeed enriched by the multiple critical levels. Our goals here are different to Leib & Goldstein's, but our asymptotic analysis has many common points. The main difference is that we study the case of a single mode bifurcating from the continuous spectrum, whereas Leib & Goldstein consider two bifurcating modes.

This article is organized as follows. In § 2 we formulate the governing equations of the problem. In § 3, we provide a detailed discussion of the linear stability problem. Section 4 is an overview of the asymptotic expansion, the details of which are given in an Appendix. Section 5 describes our exploration of the reduced model. Finally, the special reflectional symmetry of the Bickley jet allows a special class of regular neutral modes in the linear stability problem which are not a property of generic jet profiles (see § 3). To allow our analysis to be more general, we explore this issue further and introduce a slight asymmetry into the Bickley jet profile in § 6.

2. Formulation

Our goal in this article is to explore the dynamics of unstable jets in two-dimensional, incompressible fluid on the beta-plane. We are further interested in situations in which there is a basic equilibrium shear flow in the x-direction, $U(y)$; we focus on either the Bickley jet or slightly distorted variants of this flow that lack the reflectional symmetry about the jet axis. For viscous flows, these equilibria must be maintained by an external body force, which we assume given.

The dynamics of the flow is described by the vorticity, $\tilde{\omega}(x, y, t)$, and streamfunction, $\tilde{\psi}(x, y, t)$. We separate the equilibrium from any evolving perturbations by defining

$$\tilde{\psi}(x, y, t) = -\int^{y} U(y')\mathrm{d}y' + \psi(x, y, t), \quad \tilde{\omega}(x, y, t) = -U'(y) + \omega(x, y, t). \tag{2.1}$$

Then, the governing equations for the perturbations take the dimensionless form

$$\omega_t + U\omega_x + J(\psi, \omega) = \nu\nabla^2\omega + (U' - \beta)\psi_x, \tag{2.2}$$

$$\psi_{yy} + \psi_{xx} = \omega, \tag{2.3}$$

where $J(\psi, \omega) = \psi_x\omega_y - \psi_y\omega_x$, ν is a viscosity parameter (an inverse Reynolds number) and β measures the beta-effect (the background, planetary vorticity gradient).†

We assume periodic boundary conditions in x. In the cross-stream direction, we consider a variety of different configurations, ranging from infinite (in y) shear flows to bounded jets with fixed or periodic boundaries. In these cases, the streamfunction is required to be bounded, vanish or be periodic as we approach the boundaries. For viscous flows, further conditions are required on the velocity field. However, we add only weak viscosity in our analysis and the effects of viscosity become localized to the mode critical layers; the boundary conditions are effectively decoupled from these layers and we need not explicitly specify the precise conditions. In the nonlinear, viscous numerical computations, we use periodic boundary conditions (the scheme we use is described further in Appendix A).

3. Inviscid linear theory of the Bickley jet

Several previous studies (Lipps 1962; Drazin, Beaumont & Coaker 1982; Maslowe 1991) have presented inviscid linear stability calculations of the Bickley jet. In this section, we report computations that are more detailed than these previous works, and they largely unify them. The main goal is to summarize the stability characteristics

† β is not precisely the usual beta-parameter of geophysical fluid dynamics, since it is defined with reference to the basic jet profile. As a result, our jet always has one direction, but the Coriolis force changes sign with β; it is more customary in geophysical fluid dynamics to have the beta parameter positive and the jet to reverse direction.

of the basic flow in preparation for the weakly nonlinear theory. For periodic jets (in both x and y) we have verified that weak viscosity does not qualitatively affect the inviscid instability.

We pursue inviscid linear stability theory by setting $\nu = 0$, introducing the decomposition

$$\psi(x, y, t) = \hat{\psi}(y)\mathrm{e}^{\mathrm{i}k(x-ct)} + \text{c.c.}, \tag{3.1}$$

and then linearizing in the amplitude, $\hat{\psi}(y)$:

$$(U - c)(\hat{\psi}'' - k^2\hat{\psi}) = (U'' - \beta)\hat{\psi}. \tag{3.2}$$

Here, k is the streamwise wavenumber and the wave speed, $c = c_r + \mathrm{i}c_i$, is the eigenvalue of the stability problem. In unbounded cross-stream domains, the Rayleigh–Kuo equation (3.2) is solved subject to $\hat{\psi}$ remaining finite as $y \to \pm\infty$. Alternatively, in bounded domains, $-L \leqslant y \leqslant L$, we impose $\hat{\psi}(-L) = \hat{\psi}(L) = 0$ to simulate distant walls, or $\hat{\psi}(-L) = \hat{\psi}(L)$ and $\hat{\psi}_y(-L) = \hat{\psi}_y(L)$ to compare with numerical simulations.

Despite its apparently simple appearance, the eigenvalue problem in (3.2) is actually rather complicated due to the singularities that occur when c is real at the points for which $U(y) = c$. These locations are the critical levels of neutral waves, and are symptomatic of the continuous spectrum. In addition, when $\beta < 0$ there can also be a set of neutral modes with $c = c_r > 1$. These smooth eigenmodes are Rossby waves and have discrete values of c_r. There is only a finite number of these modes in a bounded channel if β is finite, and they disappear as $\beta \to 0$ (Drazin *et al.* 1982).

Neither the continuous spectrum nor the Rossby waves can directly destabilize the flow. Instead, jet instability arises from another class of smooth, discrete eigensolutions with complex values of c. Because complex solutions occur in conjugate pairs, the presence of a complex mode signifies instability. Standard manipulations on the Rayleigh–Kuo equation show that these complex modes only exist if $\beta - U''(y)$ changes sign somewhere in the domain (Kuo's generalization of Rayleigh's Theorem). This condition requires $-2 < \beta < 2/3$ for the Bickley jet. Outside this range of β, only real modes can exist (smooth Rossby waves or singular continuum modes).

When the flow is unstable, complex modes exist over certain regions of the (β, k) parameter plane. The edges of these regions are the stability boundaries; we denote their loci by $\beta = \beta_*(k)$. On approaching the stability boundaries, the complex modes smoothly limit to neutral waves with $c_i \to 0$. The limiting neutral modes are either Rossby waves with $c_r > 1$ (Drazin *et al.* 1982), or 'inflectional' modes, for which $c = U(y)$ at the same locations where $\beta = U''(y)$ (that is, the critical levels line up with the inflection points of the mean 'profile', $U - \beta y^2/2$). With that coincidence, there is no singularity in the eigenvalue equation and the solutions are smooth. Because the inflectional modes have critical levels, they may also be considered to be part of the continuous spectrum. In particular, they are the embedded neutral modes that occur when the complex pairs merge with the continuous spectrum.

For the Bickley jet, the inflectional modes can be found explicitly: we have $U(y) = \operatorname{sech}^2 y$ and $U'' \equiv 2U(2 - 3U)$, which imply that $\beta = 2c(2 - 3c)$. The Rayleigh–Kuo equation then reduces to

$$\hat{\psi}'' - k^2\hat{\psi} = (4 - 6c - 6\operatorname{sech}^2 y)\hat{\psi}. \tag{3.3}$$

With the transformation $\tau = \tanh y$,

$$(1 - \tau^2)\hat{\psi}_{\tau\tau} - 2\tau\hat{\psi}_\tau + 6\hat{\psi} - \left(\frac{k^2 + 4 - 6c}{1 - \tau^2}\right)\hat{\psi} = 0. \tag{3.4}$$

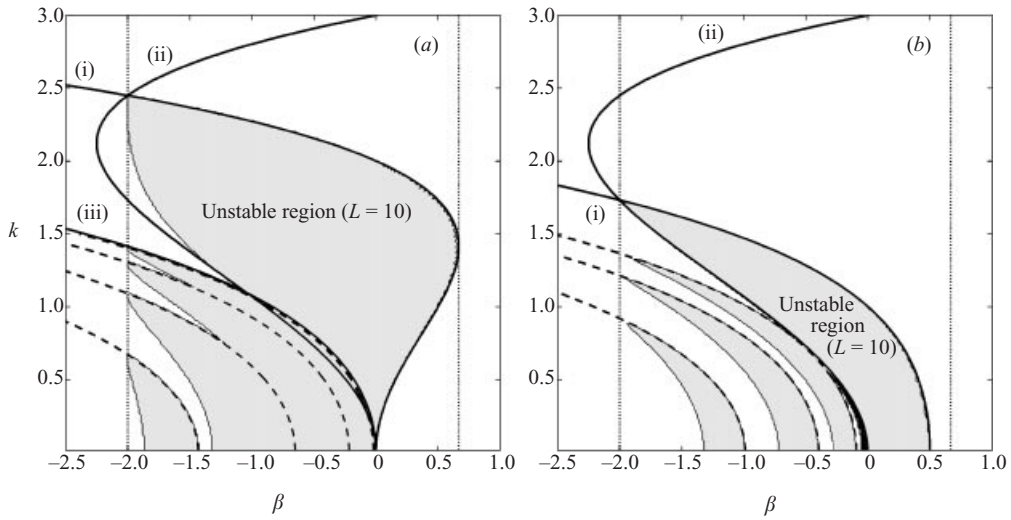

FIGURE 1. Location of neutral waves on the (β,k)-plane for (a) even modes and (b) odd modes. In (a), the curves show (i) the regular mode with $\beta = k^2(4-k^2)/6$, (ii) Howard & Drazin's singular mode with $\beta = -k^2(1-k^2/9)$, and (iii) the regular mode with $\beta = -k^2(k^2+4)/2$. In (b), the curves show (i) the regular mode with $\beta = (1-k^2)(3+k^2)/6$, and (ii) Howard & Drazin's singular mode. In both cases, the shading shows the unstable region for a bounded flow with $L = 10$, and the dashed curves indicate the inflectional modes with $\beta = 2c(2-3c)$, $k^2 = 6c-4+m^2$ and $m(L)^2 < 0$.

The solution is expressed in terms of associated Legendre functions, $aP_n^m(\tau) + bQ_n^m(\tau)$, where a and b are constants and

$$n(n+1) = 6, \quad m^2 = k^2 + 4 - 6c. \tag{3.5}$$

The imposition of the boundary conditions leads to an equation for $m(L)$. In the infinite domain, the only possible solutions have $m = 0$, 1 or 2, and $b = 0$:

$$\left.\begin{array}{cccc} \hat{\psi} = P_2^0(\tau) \equiv (3\tanh^2 y - 1)/2, & c = (k^2+4)/6, & \beta = -k^2(k^2+4)/2 & (m=0), \\ \hat{\psi} = P_2^1(\tau) \equiv \tanh y \operatorname{sech} y, & c = (k^2+3)/6, & \beta = (1-k^2)(k^2+3)/6 & (m=1), \\ \hat{\psi} = P_2^2(\tau) \equiv \operatorname{sech}^2 y, & c = k^2/6, & \beta = k^2(4-k^2)/6 & (m=2) \end{array}\right\} \tag{3.6}$$

(with $a = 1$). These solutions are all known (Lipps 1962; Maslowe 1991) their locations on the parameter plane are illustrated in figure 1.

For finite domains, provided L is sufficiently large, there are analogues of the $m = 1$ and 2 modes. These odd and even modes delineate parts of the stability boundaries of varicose and sinuous instabilities (Lipps 1962; Howard & Drazin 1964; Maslowe 1991). This is illustrated in figure 1, which displays the regions of instability of a bounded shear flow, determined numerically. The $m = 1$ and 2 inflectional modes bound the unstable ranges from above; the remaining parts of the stability boundaries are more complicated. There are also further inflectional modes with $m^2 < 0$ that are again drawn in the figure.

Also drawn in figure 1 is a singular neutral mode found by Howard & Drazin (1964) with

$$\hat{\psi} = \left|\frac{\sinh y}{\cosh^2 y}\right|^{k^2/3} \tanh^2 y, \quad c = 1, \quad \beta = -k^2\left(1 - \frac{k^2}{9}\right). \tag{3.7}$$

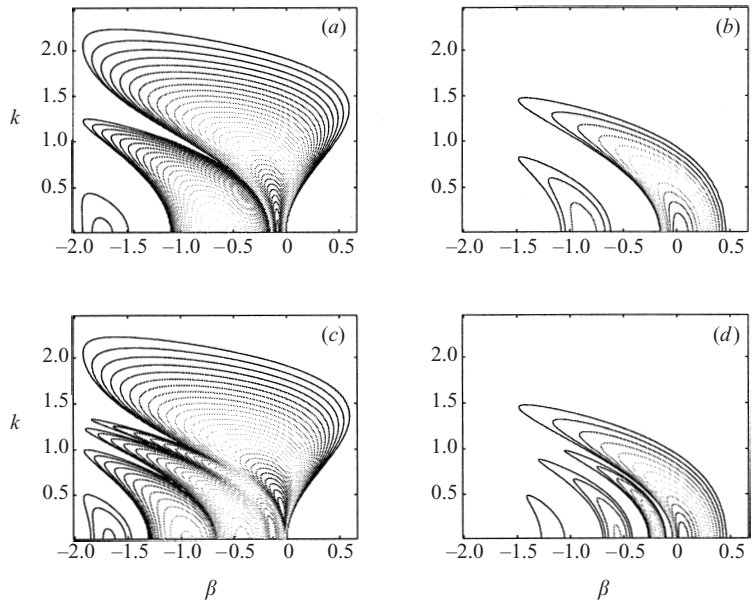

FIGURE 2. Contour plots of maximal c_i on the (β, k)-plane for a bounded jet. (a, c) The maximum values of c_i for the even, sinuous modes (corresponding to perturbations that describe meanders), and (b, d) the same for the odd, varicose modes. (a, b) $L = 5$; (c, d) $L = 10$ (the unstable regions in this case are also shown in figure 1). Contour levels are spaced by 0.01.

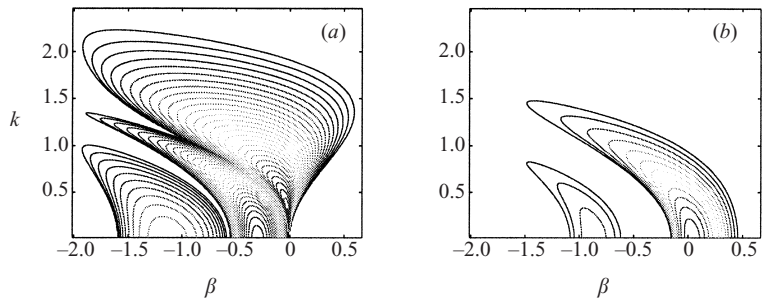

FIGURE 3. Contour plots of maximal c_i on the (β, k)-plane for a jet in a periodic domain with $L = 5$. (a) The maximum values of c_i for the sinuous modes, and (b) the same for the varicose modes. Contour levels are spaced by 0.01. Except in the regions with $k \ll 1$, the contours are essentially unchanged when we add weak viscosity, which illustrates how the inviscid instability is not qualitatively affected by viscosity in this parameter range.

Though it is not smooth, this mode appears to have some physical significance: in the infinite domain, Maslowe observed that the mode delimits a piece of the stability boundary for the odd modes. This is also suggested in figure 1(b).

Eigenvalues of complex modes, computed numerically, are shown in figures 2 and 3. Figure 2 compares the growth rates of instabilities for bounded flows in domains of different size. Results for a periodic domain are shown in figure 3. The primary instability is little different in the three cases (compare the panels for positive β, or for larger k). However, for smaller wavenumber and negative β (the lower left portion of the figures), there are significant differences. Here, the growth rates form a pattern of 'tongues': the larger the domain, the more tongues. These arise because,

away from the core of the jet, $U \to 0$ and so $\psi'' \approx (k^2 + \beta/c)\psi$. Thus, if $|c_i| \ll c_r$ and $k^2 < -\beta/c_r$, the modes are spatially oscillating, leading to a pronounced dependence on L and the type of boundary conditions. For $k^2 > -\beta/c_r$, on the other hand, the eigenfunctions decay exponentially away from the jet's core, which implies that the boundary conditions are unimportant here. Notably, this means that the upper stability boundary (for which $k^2 > -\beta$ and $c_r < 1$) is insensitive to the boundary conditions.

For both the even and odd modes, the upper pieces of each tongue of the stability boundary can be identified with an inflectional mode; see figure 1. The even modes lying along the lower boundary of each tongue have $c_r > 1$ and consequently are discrete Rossby waves (see Drazin *et al.* 1982 and Maslowe 1991). The lower boundaries of the tongues of the odd modes, on the other hand, appear to be characterized by neutral modes with $c_r = 1$ and are therefore relatives of Drazin & Howard's singular mode.

4. Scalings and the single-wave model

We now consider weakly nonlinear theory for the unstable jet. To do this, we must open an asymptotic expansion about a neutrally stable equilibrium flow. However, as found in the last section, the jet appears to be unstable for any value of β in the range $[-2, 2/3]$. Consequently, unless we focus on the marginally stable flows with $\beta = 2/3$ and -2, our only option for selecting a general basic state is to take a domain size in x for which the minimum wavenumber, k_m, lies on the upper stability boundary of the sinuous mode; that is, $k = k_m$. Thus, the $m = 2$ inflectional mode has the longest wavelength in the domain we consider, and is of special importance in the present study.

With this choice, we open the expansion with a neutrally stable Bickley jet in an infinite domain in y (as mentioned earlier, there is no essential difference for the inflectional modes if the jet is infinite, bounded or periodic in y), and set

$$U = \operatorname{sech}^2 y - c_*, \tag{4.1}$$

where $2c_*(2 - 3c_*) = \beta_*$, and $\beta_*(k)$ and $c_*(k)$ denote the position of the stability boundary for the given minimum wavenumber, k. The subtraction of the constant c_* amounts to a Galilean transformation into a frame in which the neutral mode of the jet is stationary; the flow evolves about this state on a much slower time scale. We also have $c_* = \operatorname{sech}^2 y_*$, where $y = \pm y_*$ denote the critical levels of the inflectional mode.

To capture the dynamics, we set

$$\partial_t \to \epsilon \partial_T, \quad \beta = \beta_* + \epsilon\beta_1, \quad \nu = \epsilon^3 \nu_3, \tag{4.2}$$

$$\psi = \epsilon^2 \psi_2 + \epsilon^3 \psi_3 + \cdots, \quad \omega = \epsilon^2 \omega_2 + \epsilon^3 \omega_3 + \cdots, \tag{4.3}$$

where ϵ is a small parameter that we use to order the asymptotic expansion. The scaling of ν ensures that viscous effects first appear at the same order as nonlinearity and instability. Otherwise, the particular asymptotic scheme is the same as the 'trapping scaling' of plasma physics (e.g. Crawford 1995) and is standard in critical-layer theory.

We begin the asymptotic analysis with a regular expansion using the trapping scalings. At leading order, this furnishes the neutral mode with an undetermined amplitude, $A(T)$. The goal of the expansion, as in all weakly nonlinear theories,

is to proceed to higher order and enforce solvability conditions which provide an evolution equation for $A(T)$. In the current problem this recipe fails at first order because singularities appear at the critical levels that prohibit the imposition of the solvability condition. As mentioned in the introduction, the cure for the singularities is to recognize that there are slender regions surrounding the critical levels in which the vorticity varies on a finer spatial scale (of order ϵ), and then proceed by finding another solution in these inner regions, or critical layers. The inner solutions cannot, in fact, be given in closed form; the vorticity equation remains nonlinear in the critical layers and must be solved fully. However, the inclusion of the inner solution fixes the solvability condition, yielding the desired evolution equation for $A(T)$. The details of the outer and inner expansions, the matching, and a final scaling of the resulting system are given in Appendix B. We summarize the results by quoting the final equations: because there are two critical layers, we have two inner vorticity variables, $\zeta_\pm(x, Y, T)$, defined in terms of an inner coordinate Y (measuring the fine scale on which $\zeta_\pm$ vary), where the $\pm$ refers to the critical layer at $y = \pm y_*$, respectively. These variables are coupled to the mode amplitude, which together satisfy the evolution equations

$$\partial_T \zeta_\pm + Y\,\partial_x \zeta_\pm + \varphi_x \partial_Y \zeta_\pm - \lambda \partial_Y^2 \zeta_\pm = -\gamma \varphi_x - \kappa \varphi_T, \quad \varphi(x,T) = A(T)\mathrm{e}^{-\mathrm{i}x} + \text{c.c.}, \tag{4.4}$$

$$\mathrm{i}A_T = \frac{1}{4\pi}\int_{-\infty}^{\infty}\int_0^{2\pi} \mathrm{e}^{-\mathrm{i}x}(\zeta_+ + \zeta_-)\,\mathrm{d}x\mathrm{d}Y \equiv \tfrac{1}{2}\langle \mathrm{e}^{-\mathrm{i}x}(\zeta_+ + \zeta_-)\rangle, \tag{4.5}$$

where λ, γ and κ are parameters ($\lambda \propto \nu_3$ is a new viscosity, γ is a scaled version of the control parameter β_1, and κ is determined by the background flow profile, $\kappa \propto U'''(y_*)/U'(y_*)^2$). φ denotes the leading-order streamfunction which is the same inside each critical layer, and k has now been scaled out. The right-hand side of the first relation in (4.4) represents the advection of the background vorticity field inside the critical layers by the mode. The equations are solved subject to the boundary conditions, $\zeta_\pm \to (\kappa\varphi_{Tx} - \gamma\varphi)/Y$ as $|Y| \to \infty$, and the integrals over Y in (4.5) must be interpreted in terms of principal values at their limits.

Because of the form of (4.4), it is convenient to define the even and odd vorticity components, $\zeta_e = (\zeta_+ + \zeta_-)/2$ and $\zeta_o = (\zeta_+ - \zeta_-)/2$. The odd component satisfies

$$\partial_T \zeta_o + Y\,\partial_x \zeta_o + \varphi_x \partial_Y \zeta_o - \lambda \partial_Y^2 \zeta_o = 0. \tag{4.6}$$

Thus, if ζ_o is initially zero, then it remains so throughout the evolution. Even if this component is not initially zero, it does not couple to the mode amplitude. Hence we ignore this component hereafter, and set $\zeta = \zeta_e$, which leaves the system

$$\zeta_T + Y\zeta_x + \varphi_x \zeta_Y - \lambda \zeta_{YY} = -\gamma\varphi_x - \kappa\varphi_T, \quad \mathrm{i}A_T = \langle \mathrm{e}^{-\mathrm{i}x}\zeta\rangle, \tag{4.7}$$

$$\varphi = A\mathrm{e}^{-\mathrm{i}x} + \text{c.c.}, \quad \zeta \to (\kappa\varphi_{Tx} - \gamma\varphi)/Y \quad \text{as} \quad |Y| \to \infty. \tag{4.8}$$

These coupled equations are identical to those derived for a mode with a single critical layer (Churilov & Shukhman 1987; Goldstein & Leib 1988; Goldstein & Hultgren 1998). Thus, although there are two critical layers, the dynamics is no richer. As we see in § 6, this remains true even if the profile is made slightly asymmetrical.

5. Dynamics of the single-wave model

5.1. *Properties of the model*

The single-wave model arises in various shear flow problems (Churilov & Shukhman 1987, Balmforth 1999), for disturbed vortices (Balmforth *et al.* 2000), and in plasmas

(del Castillo-Negrete 1998). This underscores the fact that this model describes a particular kind of transition to instability (the bifurcation of a mode from a continuous spectrum), yet there are relatively few systematic discussions of its solutions beyond some asymptotic limits. In fact, we are aware of no solutions other than a handful presented by Goldstein and collaborators (Goldstein & Leib 1988; Goldstein & Hultgren 1998) for unstable modes, and Balmforth *et al.* (2000) for forced stable modes, and some computations reported in plasma physics for a related, but different model (O'Neil *et al.* 1971; Onishchenko *et al.* 1971; Tennyson *et al.* 1994). For this reason, we dwell in some detail on the dynamics of the single-wave model.

We begin by mentioning some general properties of the model. First, there are three parameters in the equations: γ, κ and λ. As indicated in Appendix B, we may take $|\gamma| = 1$ (unless $\beta_1 = 0$); as shown below, if $\gamma = -1\,(+1)$, the system is unstable (stable). Only two positive parameters then remain ($\lambda \geqslant 0$ because the viscosity is positive, and $\kappa \geqslant 0$ because changing the sign of this parameter amounts to a reflection of the spatial coordinates). As described in Appendix C, if either of the two parameters becomes large, the system can be asymptotically reduced to an ordinary differential equation for the mode amplitude, $A(T)$. This dimensional reduction occurs because the two limits are both characterized by significant dissipation.

Second, the model has a number of global conservation or balance laws:

$$\frac{\mathrm{d}}{\mathrm{d}T}\langle\zeta\rangle = 0, \quad \frac{\mathrm{d}}{\mathrm{d}T}(|A|^2 - \langle Y\zeta\rangle) = 0, \quad \frac{\mathrm{d}}{\mathrm{d}T}\langle\Psi\zeta - \kappa|A|^2\rangle = \lambda\langle\zeta\rangle, \tag{5.1}$$

$$\frac{\mathrm{d}}{\mathrm{d}T}(\gamma|A|^2 + \tfrac{1}{2}\langle\zeta^2\rangle) = -\lambda\langle\zeta_Y^2\rangle, \tag{5.2}$$

where $\Psi = Y^2/2 - \varphi$ is the total streamfunction. The integrals in these relations all converge provided one performs the integral in x first. The first two relations correspond to conservation of the mean critical-layer vorticity and momentum. The second two relations are energy and enstrophy equations (for the energy relation, the subtraction of $\kappa|A|^2$ from $\Psi\zeta$ ensures that the integral converges, assuming that $\zeta \sim (\kappa\varphi_{Tx} - \gamma\varphi)Y^{-1} + (\kappa|A|^2 - \kappa\varphi_{TT} - \gamma\varphi_{Tx})Y^{-2}$). When $\lambda = 0$, there is also an infinite number of Casimir invariants, $\langle F(q)\rangle$, given by any function, $F(q)$, of the total vorticity, $q = \zeta + \kappa\varphi + \gamma y - \kappa y^2/2$.

Finally, we are interested in the nonlinear dynamics of unstable modes, rather than how vorticity perturbations are rearranged within the critical layers. A suitable initial condition is then

$$A(T = 0) = A_0, \quad \zeta(x, Y, T = 0) = 0, \tag{5.3}$$

for some small initial amplitude A_0. In numerical computations, we take $A_0 = 10^{-3}$ and solve the equations using the operator-splitting scheme described in Appendix A.

5.2. *Linear theory*

5.2.1. *Inviscid normal modes*

The linear dynamics of the perturbed neutral mode can be discussed straightforwardly within the framework of the single-wave model. First, consider inviscid normal modes with dependence $\exp \mathrm{i}(x - c_1 T)$. Then,

$$\zeta = \frac{(\kappa c_1 - \gamma)\varphi}{Y - c_1}, \tag{5.4}$$

$$c_1 = \left[\pi\kappa - \frac{\mathrm{i}\,\mathrm{sgn}(c_{1i})}{1 + \pi^2\kappa^2}\right]\pi\gamma. \tag{5.5}$$

The flow is therefore unstable when $\gamma < 0$.† When $\gamma > 0$, (5.5) is not consistent and there is no normal mode; the flow is stable. The non-analyticity of the dispersion relation (the appearance of $\mathrm{sgn}(c_{1i})$) reflects the presence of the continuous spectrum.

5.2.2. *Viscous modes*

The viscous normal modes solve

$$\lambda\zeta_{YY} + \mathrm{i}(Y - c_1)\zeta = \mathrm{i}(\kappa c_1 - \gamma)\varphi. \tag{5.6}$$

The solutions can be given in terms of Airy functions or via Fourier transforms (see Balmforth 1998). Thence,

$$c_1 = \left(\frac{\pi\kappa - \mathrm{i}}{1 + \pi^2\kappa^2}\right)\pi\gamma, \tag{5.7}$$

which is identical to the inviscid dispersion relation, save that $\mathrm{sgn}(c_{1i})$ no longer appears. (Curiously, neither does the viscosity parameter, λ.)

5.2.3. *The initial-value problem*

The initial-value problem has solution,

$$A = A_0\mathrm{e}^{\Gamma T}, \quad \zeta = \frac{\mathrm{i}\gamma A_0}{(\pi\gamma - \pi\kappa Y - \mathrm{i}Y)}(\mathrm{e}^{\Gamma T} - \mathrm{e}^{-\mathrm{i}YT})\mathrm{e}^{\mathrm{i}x} + \mathrm{c.c.}; \tag{5.8}$$

$\Gamma = \pi\gamma/(\mathrm{i}\pi\kappa - 1)$ is the viscous normal-mode eigenvalue.

These results illustrate two important features of the linear problem. First, if the system is unstable, the inviscid and viscous normal modes coincide with one another and with an exponentially growing disturbance in the initial-value problem. Second, if the system is stable, there are no inviscid eigenvalues, but there is a viscous mode and a corresponding exponentially decaying disturbance in the initial-value problem. The latter is a 'Landau pole' or a 'quasi-mode' (in the terminology of plasma physics), that one can uncover by analytical continuation of the dispersion relation. It is somewhat surprising that this quasi-mode corresponds to a viscous eigenvalue, but this result is also found in other contexts (Balmforth 1999).

5.3. *Cat's eye phenomenology*

To illustrate the nonlinear dynamics of an unstable jet we take $\gamma = -1$ and $\kappa = \lambda = 0$. The evolution of the vorticity field and mode amplitude from the initial condition (5.3) is shown in figure 4. The mode amplitude grows exponentially (with the linear growth rate) until the instability saturates. Then $|A(T)|$ begins to oscillate, or 'bounce', aperiodically about the saturation level; these bounces are equivalent to the 'trapping oscillations' of plasma theory. Simultaneously, the vorticity distribution inexorably twists up into a cat's eye pattern.

If $\kappa = 0$, and with the current initial condition, the system has the reflection symmetry $(x, Y) \to (-x, -Y)$, $\zeta \to -\zeta$ and $A \to -A^*$. Consequently, the vorticity distribution evolves into a stationary cat's eye pattern centred at $Y = 0$, as seen in figure 4. In figure 5 we show another example with $\kappa = 1/4$. In this case, the symmetry is lost and a propagating cat's eye pattern emerges.

† If we return to the original variables, as described in Appendix B.4, and take $c_{1i} > 0$, we find $c_1 = [2 + c_*(1 - c_*)^{-1/2}(\log K + \mathrm{i}\pi)]\beta_1\{4c_*[-6 + (1 - 3c_*)(1 - c_*)^{-1/2}(\log K + \mathrm{i}\pi)]\}^{-1}$, with K given in (5.9), which is the formula derived by Lipps using Tollmein–Lin perturbation theory.

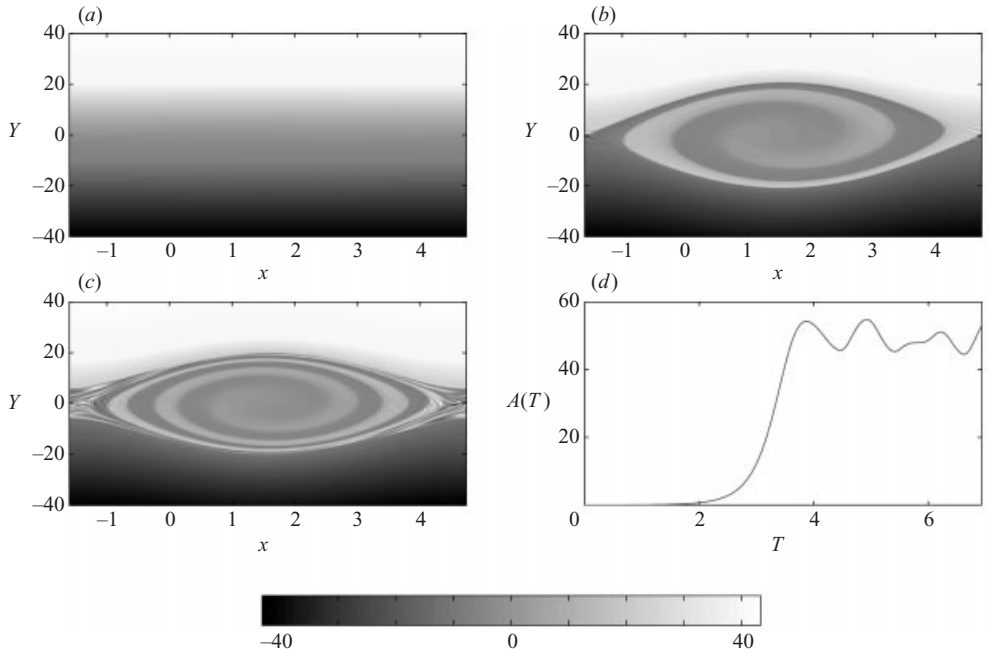

FIGURE 4. Cat's eye pattern formed from the growth of an unstable mode ($\gamma = -1$, $\kappa = 0$, $\lambda = 0$): snapshots at (*a*) $T = 2$, (*b*) 4, (*c*) 6, of the total vorticity, $q = \zeta - Y$, as densities on the (x, Y)-plane, using the grey-scale shown. (*d*) The mode amplitude.

Although there are similarities in the way that the vorticity distribution twists up in figures 4 and 5, the amplitude reached by the mode is rather different. In fact, the saturation value decreases rapidly with κ. We quantify this observation by recording the amplitude of the first bounce in $|A(T)|$ as a function of κ; see figure 6. These measurements also allow one to estimate the saturation level, given the particular value of κ suitable to a certain problem. For example, for the Bickley jet,

$$\kappa = -\left[6\frac{\sqrt{1-c_*}}{3c_*-1} + \log K\right]^{-1}, \quad K(c_*) = \frac{1+\sqrt{1-c_*}}{1-\sqrt{1-c_*}}. \tag{5.9}$$

Note that $\kappa = 0$ for $c_* = 1/3$ or $\beta_* = 2/3$, which corresponds to the rightmost point of the stability boundary in figure 1 (also, $\kappa = 1/4$ for $\beta_* \approx 0.3$ or -0.2). However, the disappearance of κ is the only feature that distinguishes this point of marginal stability in the single-wave model.

The examples above illustrate the nearly inviscid dynamics captured by the single-wave model. More dissipative cases are shown in figure 7, and reveal an important feature of the model: as the viscosity λ increases, the amplitude of the mode drifts increasingly quickly from the initial saturation value and diverges. Further asymptotic analysis (Churilov & Shukhman 1987; Goldstein & Hultgren 1988) indicates that the mode amplitude eventually grows with dependence $(\lambda T)^{2/3}$ (see Appendix C). The drift is associated with the viscous spreading of the vorticity within the critical layer (Brown & Stewartson 1978) and reflects how the dissipative cat's eye pattern is a purely ephemeral structure.

For smaller viscosities and over shorter times, the mode saturates without significant drift. The main dissipative effect in this regime is to attenuate the amplitude bounces

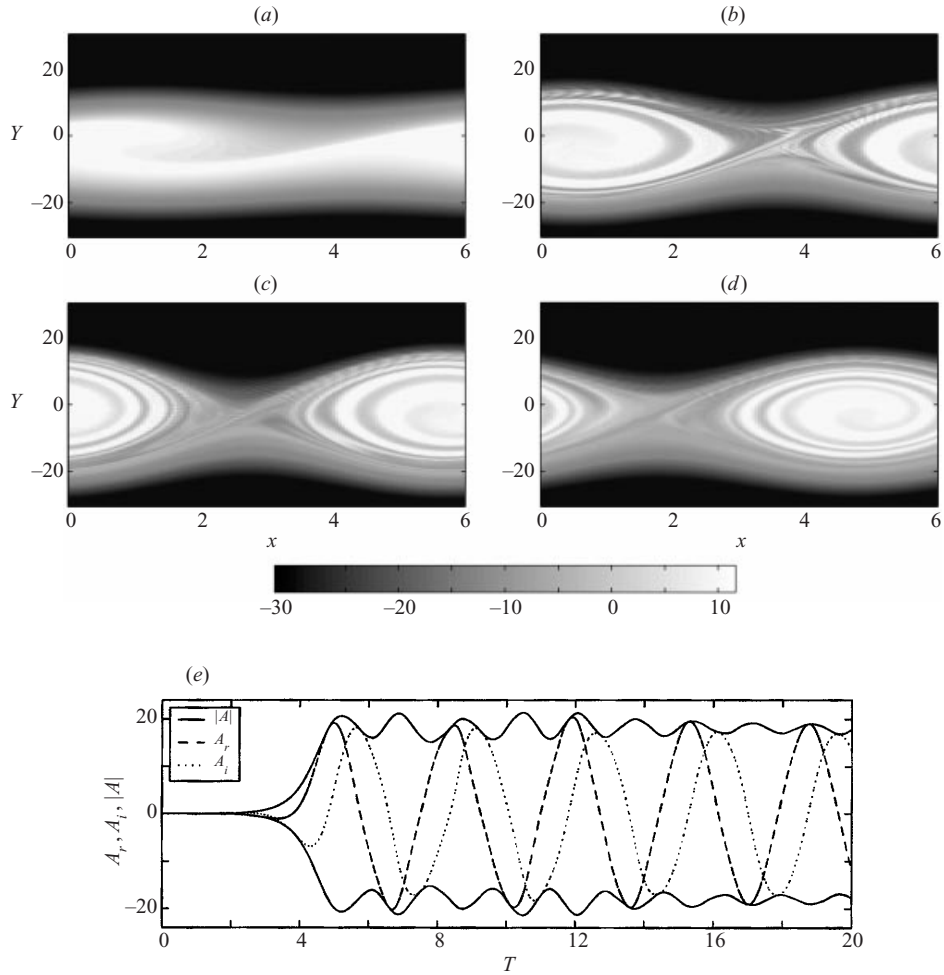

FIGURE 5. Cat's eye pattern for $\gamma = -1$ and $\kappa = 0.25$: snapshots at (*a*) $T = 4$, (*b*) 8, (*c*) 12, (*d*) 16, of the total vorticity, $q = \zeta + \kappa\varphi - Y - \kappa Y^2/2$, as densities on the (x, Y)-plane, using the grey-scale shown. (*e*) $A = A_r + \mathrm{i}A_i$. $\lambda = 10^{-4}$.

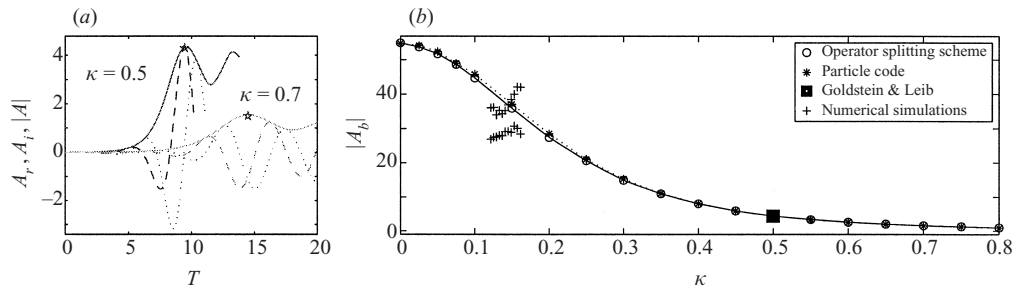

FIGURE 6. First bounce amplitude. (*a*) The definition. (*b*) As a function of κ: the circles show measurements taken using the operator splitting scheme (with $\lambda = 0$), the stars indicate analogous measurements using a particle scheme (see Appendix A), and the square at $\kappa = 1/2$ represents a value computed by Goldstein & Leib (1988). The crosses show data from numerical simulations of the original governing equations (see § 5.5); these data are plotted in a different way in figure 12. The two groups of crosses correspond to the cases with low and high viscosity respectively. The bounce amplitude is falling roughly exponentially with κ on the right of the picture.

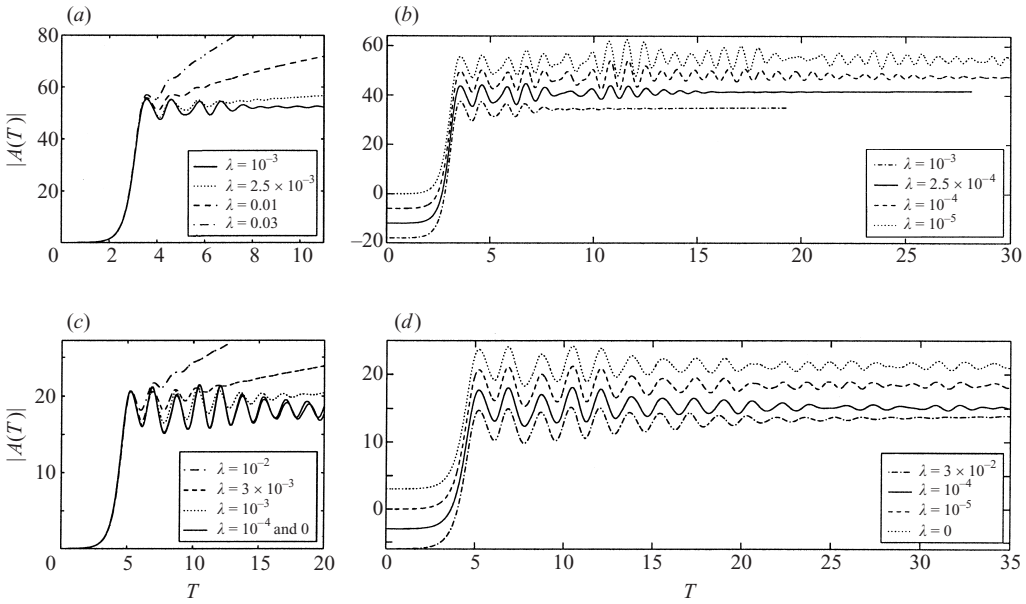

FIGURE 7. Mode amplitudes, $|A(T)|$, with time for different values of λ with $\kappa = 0$ in (a, b), and $\kappa = 1/4$ in (c, d). In (b, d), curves are successively offset for clarity.

(see figure 7). This eliminates any complex temporal dynamics associated with those oscillations and drives the system to a quasi-steady, slowly spreading state. Further details of such a state with $\kappa = 0$ are shown in figure 8. The condition of quasi-steadiness requires that the total vorticity, $q = \zeta - Y$, become a function of the streamfunction, $\Psi = Y^2/2 - \varphi$, and symmetry demands that $q = 0$ within the cat's eye; this is illustrated in figure 8(a). Note also the ridge, or ring-like 'defect', in the vorticity distribution (panels (b) and (c)), which is also associated with the relatively large spread of (Ψ, q)-points near $\Psi = -60$, and reflects a residual, faster temporal variation.

5.4. *Amplitude bounces*

The amplitude bounces begin when the core of the cat's eye first overturns into a vortex. The subsequent train of amplitude oscillations is intimately connected to deformations of this vortex. The deformations appear to have some common features with the vortex nutations seen in shear-layer computations (Miura & Sato 1978), but there are also important differences. In particular, the vortex appears sporadically to lose stability and generate non-axisymmetrical structure. For $\kappa = 0$, the bounces seem largely due to the formation and subsequent decay of elliptical deformations such as the ring-like vorticity defect in figure 8. For $\kappa \neq 0$ on the other hand, a secondary vortical structure, or satellite, develops inside the cat's eye (see figure 9), which has some analogy with the 'macro-particle' phenomenology of plasma theory (Tennyson *et al.* 1994).

As we lower the viscosity in the computations, the bounces become increasingly prolonged. Moreover, in computations in which we attempted to minimize the dissipation, the bounces appeared to continue indefinitely (see figure 10). These computations consisted of a series of high-resolution runs with both the operator-splitting scheme and a symplectic particle scheme (see Appendix A). Unfortunately,

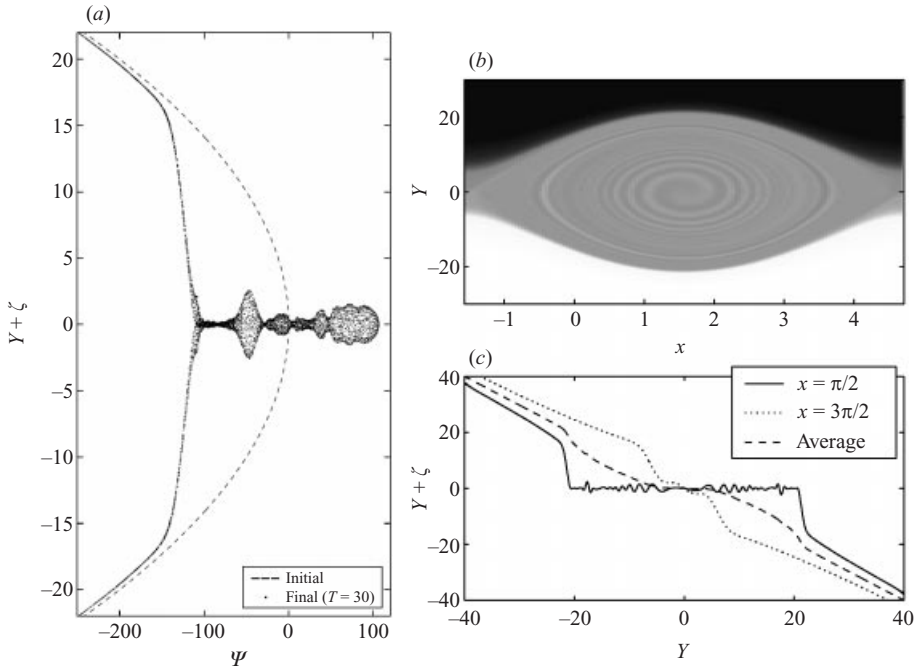

FIGURE 8. Further details of the solution with $\kappa = 0$ and $\lambda = 10^{-4}$. (a) Total streamfunction, $\Psi = Y^2/2 - \varphi$, against total vorticity, $q = \zeta - Y$, at a selection of points at $T = 30$; the dashed line is the initial condition. (b, c) More details of the vorticity distribution.

the code suffers from an intrinsic dissipation arising through the finite resolution in Y, which becomes particularly severe as the vorticity distribution twists up. Thus, as we lower the explicit viscosity, we ultimately enter a regime in which the intrinsic dissipation dominates the explicit one. Also, although the particle scheme does not suffer from limited resolution, the fine spatial scales generated in the particle distribution function eventually become smaller than the inter-particle separations. Therefore, the particle scheme also breaks down because it fails to reproduce the dynamics of the partial differential equation. Consequently, we cannot truly say from the numerical results whether the amplitude bounces are a recurrent inviscid phenomenon.

Amplitude bounces will not persist if the structures within the cat's eye are continually sheared away as the vorticity distribution twists up (O'Neil *et al.* 1971). However, such decay only proceeds if the sheared vorticity filaments are of sufficiently low amplitude; stronger structures within the cat's eye can resist the shearing process, much as Landau damping halts in a plasma when the initial amplitude exceeds a threshold (Manfredi 1997), or in vortices disturbed by sufficiently strong perturbations (Balmforth *et al.* 2000). Moreover, shearing action may be irrelevant if the bounces originate from sporadic secondary instabilities of the cat's eye.

5.5. *Numerical computations with the governing equations*

To complement the asymptotic analysis we solve the original governing equations (2.2)–(2.3) numerically, as described in Appendix A. We initialize the computation with a background jet in a domain whose size places the system just below the upper stability boundary, and then add a low-amplitude perturbation with the

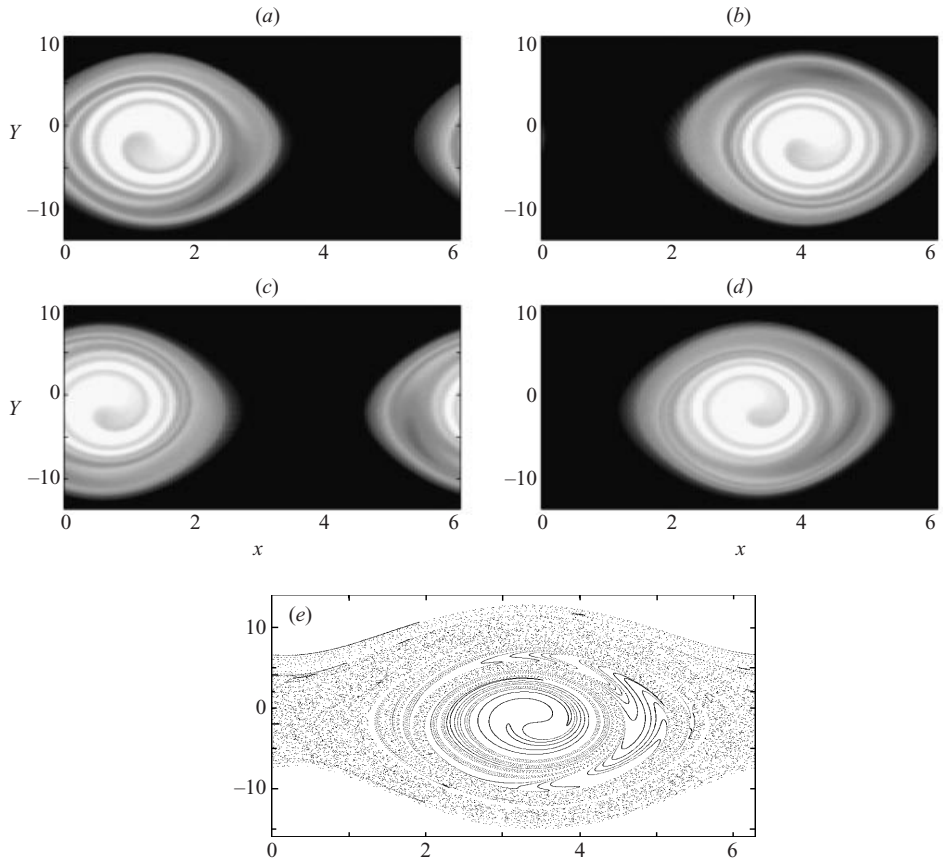

FIGURE 9. Structures inside the cat's eye in a simulation with $\kappa = 1/4$ and $\lambda = 10^{-5}$. (*a–d*) Snapshots of the total vorticity distribution at successive instants $T = 32$, 34, 36 and 38. The shading is chosen to highlight the core of the cat's eye and the secondary structure that orbits around it. (*e*) The locations at $T = 38$ of Lagrangian tracers that were initially placed at time $T = 4$ along the lines $Y = 0, \pm 3$ and ± 6.

form of the unstable mode. Results for $\beta = 0$ are shown in figures 11–13. Figure 11(*a*) shows a snapshot of the vorticity field at a time after the mode has reached an initial saturation level, ω_*, which is identified from a time series of the vorticity at a central point of the jet ($x = y = 0$) – see figure 11(*b*). Figure 12 shows how ω_* varies with k, and confirms the trapping scaling followed by the equilibrated mode.†

More quantitatively, we convert the data of figure 12 into equivalent measurements of $(\kappa, |A_b|)$ using the scalings of Appendix B.4. Those measurements are directly compared with the asymptotic theory in figure 6. Though the data from the full numerical computations are strongly influenced by the viscosity, and are taken at values of ϵ that are not that small, the saturation values are in rough agreement.

The temporal dynamics of the unstable meander is also similar to the predictions of the single-wave model: the vorticity time series in figure 11(*b*) and in figure 13

† The asymptotic theory predicts that the amplitude saturates at the level ϵ^2, where $\epsilon^2 = (\beta - \beta_*)^2$ or, equivalently, $(2-k)^2$ if we fix $\beta = 0$ and instead vary k from its critical value. For a very viscous jet, the amplitude saturates at the level, $(2-k)^{1/2}$, which is often called 'Hopf scaling'.

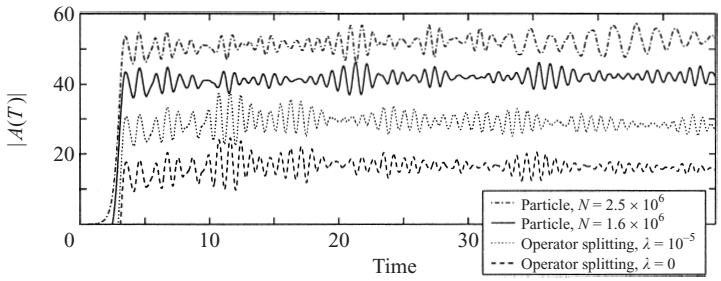

FIGURE 10. Mode amplitudes over longer times for different computational runs with $\kappa = 0$. Two runs with the operator-splitting scheme are shown, with two different values of λ, and two runs using the particle scheme with different numbers of particles. Curves are successively offset for clarity.

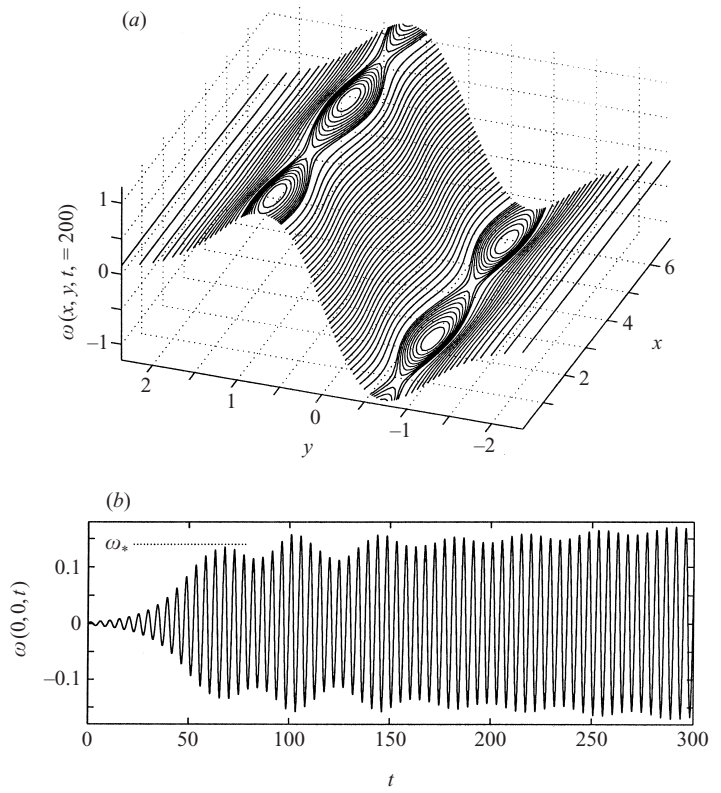

FIGURE 11. Cat's eye pattern formed from the growth of an unstable mode in a simulation of the full jet with $k = 1.8$ and $\beta = 0$ ($\nu = 3.75 \times 10^{-5}$). (*a*) A snapshot of the vorticity field; contour levels are unequally spaced and chosen to highlight the cat's eyes. (*b*) The time series of the vorticity at $(x, y) = (0, 0)$, together with ω_*, the amplitude of the first 'bounce'.

show initial linear growth, subsequent saturation and the onset of amplitude bounces, together with a viscous drift. Ultimately, the drift subsides and gives way to a slower decay originating from the viscous damping of the jet profile itself. This last stage of the evolution is not captured by the single-wave model, and is similar to the final stages of the mixing-layer instability described by Goldstein & Hultgren (1988).

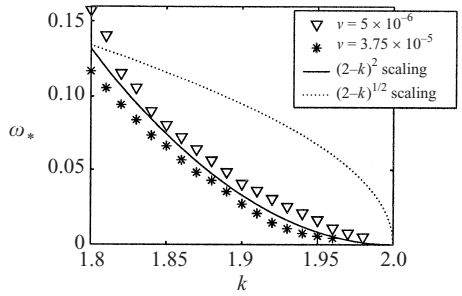

FIGURE 12. Scaling data for the Bickley jet with $\beta = 0$. Shown is ω_* with k for two values of the viscosity. The trend of the trapping scaling is also shown, for which the saturation level is order $(2-k)^2$. The 'Hopf scaling', characterized by saturation levels of order $(2-k)^{1/2}$, is the scaling one expects for instabilities with significant viscosity. The data for $1.8 \leqslant k \leqslant 1.9$ are replotted in figure 6 using the rescalings of Appendix B.4

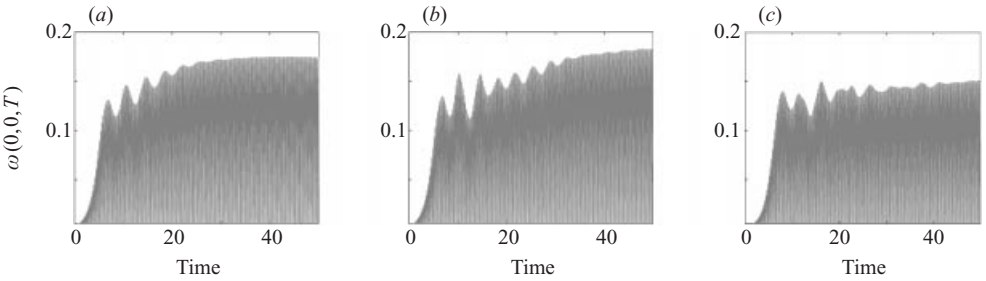

FIGURE 13. Time series of the vorticity at $(x, y) = (0, 0)$ for (a) $\nu = 3.75 \times 10^{-5}$, (b) $\nu = 5 \times 10^{-6}$ and (c) $\nu = 10^{-6}$.

Computational limitations preclude a more demanding comparison of the numerical simulations of the full equations with the single-wave model: even with 512 Fourier modes in y, each critical layer has effectively only about 40 grid points. By contrast, in solving the single-wave model, we place over a thousand grid points inside the critical layer in order to resolve the twist-up of the vorticity field for as long as possible. Even in a model of an unstable shear layer with only a single critical layer, there would still be a factor of ten difference in resolution. In other words, with moderate computational resources, the numerical simulations of the full equations cannot adequately approach the critical-layer limit, a fact that we could have cited as motivating the single-wave model at the outset. It remains to be seen whether a numerical scheme with an adaptive, highly stretched mesh could perform better.

6. Asymmetrical jets

The expansion of the previous section highlights the special importance of inflectional modes (the smooth, discrete eigensolutions that delineate the upper stability boundary). However, these modes cannot be a generic feature of jets because the levels for which $U'' = \beta$ do not, in general, have the same mean flow speed. The Bickley jet supports these modes because it has reflection symmetry about $y = 0$ and therefore satisfies this condition automatically. However, the non-genericity of the inflectional modes brings into question the usefulness of the analysis presented above. To address this issue, we now consider what happens to these special neutral modes when we break the symmetry of this particular profile.

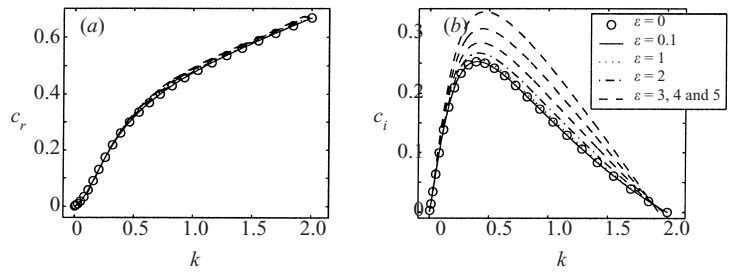

FIGURE 14. Plots of (a) c_r and (b) c_i against k for the sinuous modes of asymmetrical jets with $\beta = 0$ and various values of ε. The symmetrical case is shown by the circles.

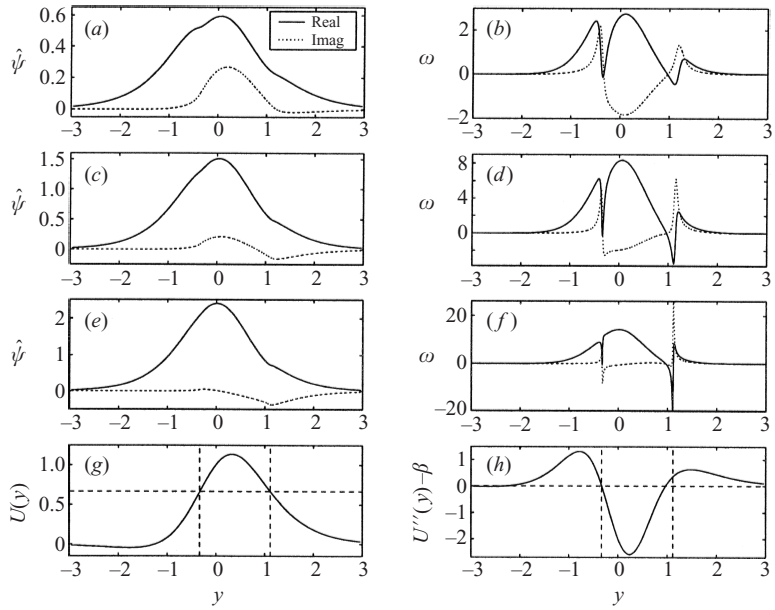

FIGURE 15. Eigenfunctions of an asymmetrical, bounded jet. $L = 5$, $\beta = 0$ and $\varepsilon = 1$. Streamfunction (left) and vorticity perturbations (right) for (a, b) $k = 1.6$, (c, d) $k = 1.8$ (e, f) $k = 1.9$. (g) The profile itself, and (h) the mean, total vorticity gradient, $U'' - \beta$. The dashed lines show the position of the critical layers as k limits to the stability boundary.

By way of example, we consider the flow with

$$U(y) = (1 + \varepsilon y)\,\mathrm{sech}^2 y \tag{6.1}$$

and $\beta = 0$. A set of eigenvalues for different ε are displayed in figure 14. Even with strong asymmetry, the eigenvalues appear much like those of the symmetrical jet and disappear near $k = 2$. However, the limiting neutral eigenmodes cannot be smooth. Indeed, a progression of eigenfunctions as k tends to the stability boundary is shown in figure 15; the eigenfunctions develop sharp peaks as $c_i \to 0$, suggesting that the limiting eigenfunctions are singular (see also Howard 1964).

To explore the dynamics of asymmetrical jets from an analytical perspective we introduce a weak asymmetry into the basic profile and continue again down the route outlined in Appendix B. This time we set

$$U = \mathrm{sech}^2 y - c_* + \epsilon f(y), \tag{6.2}$$

where $f(y)$ is an antisymmetric function about $y = 0$. We then derive the system (see Appendix B)

$$\partial_T \zeta_e + Y\,\partial_x \zeta_e + \varphi_x \partial_Y \zeta_e - \lambda \partial_Y^2 \zeta_e = -\gamma \varphi_x - \kappa \varphi_T, \tag{6.3}$$

$$\partial_T \zeta_o + Y\,\partial_x \zeta_o + \varphi_x \partial_Y \zeta_o - \lambda \partial_Y^2 \zeta_o = \sigma \varphi_x, \tag{6.4}$$

$$\mathrm{i}A_T = \langle \mathrm{e}^{-\mathrm{i}x} \zeta_e \rangle, \quad \varphi = A\mathrm{e}^{-\mathrm{i}x} + \text{c.c.}, \tag{6.5}$$

where σ is a measure of the asymmetry of the flow profile. Though the odd vorticity component is now forced, the mode still couples only with the even component, and the (A, ζ_e) subsystem is identical to the single-wave model. This signifies that the asymmetrical distortion of the mean flow induces an antisymmetrical vorticity component but does not change the modal dynamics. Also, when $\kappa = 0$, the two evolution equations are identical up to scaling by $-\sigma/\gamma$. Hence, for these parameter values, and initial conditions permitting, the two fields evolve in identical fashions.

The inviscid normal modes predicted by (6.3)–(6.5) are

$$\zeta_e = \frac{(\kappa c_1 - \gamma)\varphi}{Y - c_1}, \quad \zeta_o = \frac{\sigma \varphi}{Y - c_1}. \tag{6.6}$$

Moreover, the dispersion relation is unchanged from the symmetrical case. Notably, when $\gamma = 0$, the flow is neutrally stable and we are positioned at a point on the upper stability boundary. In this instance,

$$\zeta_e = 0, \quad \zeta_o = \frac{\sigma \varphi}{Y}. \tag{6.7}$$

Thus the neutral mode is singular, as suggested by the numerical results described above.

With dissipation, the asymmetrical vorticity component of the normal mode satisfies

$$\lambda \zeta_o'' + \mathrm{i}(Y - c_1)\zeta_o = \mathrm{i}\sigma \varphi. \tag{6.8}$$

Hence,

$$\zeta_o = \mathrm{i}\pi\sigma\varphi \int_0^\infty \exp(-\lambda q^3/3 + \mathrm{i}q(y - c_1))\,\mathrm{d}q, \tag{6.9}$$

which indicates that the eigenfunctions become smooth with viscosity.

With $A(0) = A_0$ and $\zeta_e(x, Y, 0) = \zeta_o(x, Y, 0) = 0$, the solution of the initial-value problem is given by

$$A = A_0 \mathrm{e}^{\Gamma T}, \tag{6.10}$$

$$\zeta_e = \frac{\mathrm{i}\gamma A_0}{(\pi\gamma - \pi\kappa Y - \mathrm{i}Y)} (\mathrm{e}^{\Gamma T} - \mathrm{e}^{-\mathrm{i}Y T}) \mathrm{e}^{\mathrm{i}x} + \text{c.c.} \tag{6.11}$$

and

$$\zeta_o = -\frac{\mathrm{i}\sigma(1 - \mathrm{i}\pi\kappa)A_0}{(\pi\gamma - \pi\kappa Y - \mathrm{i}Y)} (\mathrm{e}^{\Gamma T} - \mathrm{e}^{-\mathrm{i}Y T}) \mathrm{e}^{\mathrm{i}x} + \text{c.c.} \tag{6.12}$$

For neutrally stable jets, $\Gamma = 0$, $A = A_0$, $\zeta_e = 0$ and

$$\zeta_o = -\frac{2\sigma}{Y} A_0 [\cos x - \cos(x - Y T)]. \tag{6.13}$$

Although this solution is non-singular, there is a resonant response at the critical level $Y = 0$, where the mode amplitude grows linearly with time. At some stage, the solution must therefore break out of the linear regime and enter a nonlinear state.

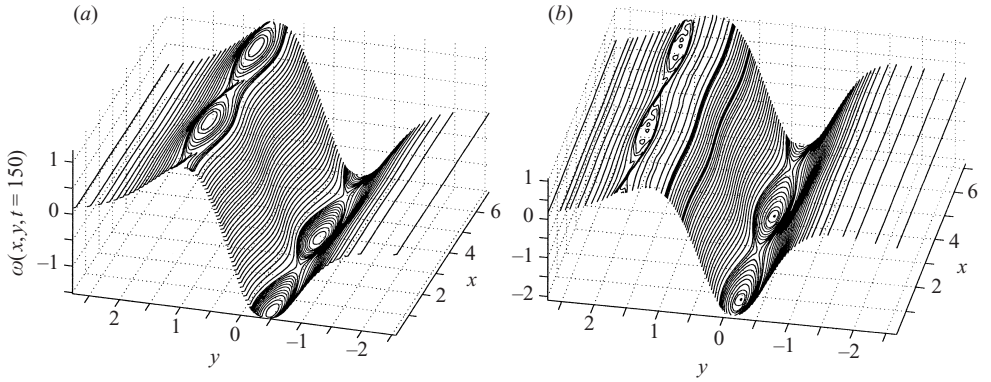

FIGURE 16. Cat's eye patterns formed from the growth of an unstable mode in a simulation of an asymmetrical jet. The mean profile is given by (6.1) with (*a*) $\varepsilon = 0.8$ and (*b*) $\varepsilon = 3$, and $k = 1.8$ and $\beta = 0$. Shown are snapshots of the vorticity field at $t = 150$.

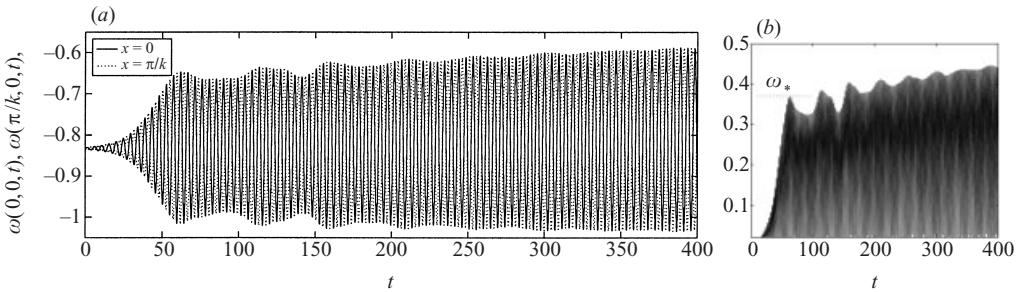

FIGURE 17. (*a*) Time series of the vorticity at $(x, y) = (0, 0)$ and $(x, y) = (\pi/k, 0)$ for the simulations of figure 16(*a*). (*b*) The magnitude of the differences of these series and a slightly different definition of the saturation value, ω_*. This definition is not completely free from ambiguity for some of the computations, but it is computationally convenient.

The nonlinear solution satisfies the equation

$$\partial_T \zeta_o + Y \partial_x \zeta_o - 2\partial_Y \zeta_o \sin x = -2A_0 \sigma \sin x, \tag{6.14}$$

which can be solved by the method of characteristics (O'Neil 1965; Stewartson 1978), and indicates that the vorticity distribution again twists up into a cat's eye pattern.

Numerical results for asymmetrical jets in the full problem are shown in figures 16–18 (again we choose $\beta = 0$ for illustration). In figure 16, we show snapshots of the vorticity field in runs with different asymmetry parameters ($\varepsilon = 0.8$ and 3). The snapshot for $\varepsilon = 0.8$ shows mild asymmetries, but the vorticity field is strongly skewed for $\varepsilon = 3$. So much so, in fact, that one cat's eye structure completely dominates the other and displaces it from the vorticity extremum. However, in both cases, the mode amplitude evolves in much the same way as for the symmetrical jet: there are irregular amplitude bounces and a slow viscous drift (see figure 17). The dependence of the saturation level on k is also hardly changed by the skewing of the mean vorticity (figure 18).

In summary, because the asymptotic theory builds on the single-wave model without qualitatively modifying it, we conclude that the symmetry of the Bickley jet is not an essential requirement to the dynamics we predict at the onset of instability.

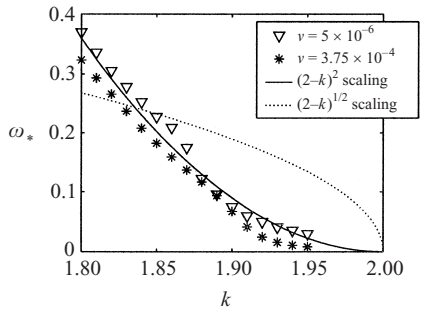

FIGURE 18. Saturation level, ω_* (defined as in figure 17), against k for asymmetrical jets with $\beta = 0$, $\varepsilon = 0.8$ and two values of the viscosity. The trends of trapping and Hopf scalings are also shown (respectively, $(2-k)^2$ and $(2-k)^{1/2}$).

7. Summary

In this study we have explored weakly unstable, almost inviscid meanders of two-dimensional jets on the beta-plane. We began with linear stability theory for the Bickley jet, and outlined a weakly nonlinear theory for a particular mode of instability. This 'inflectional' mode is a smooth, discrete eigenmode whose critical layers line up with the extremal points of the mean, total vorticity. Finally, we considered slightly asymmetrical jets in order to gauge how the dynamics changed when the neutral inflectional modes were no longer smooth.

The weakly nonlinear theory for the unstable inflectional modes furnishes a reduced model also derived in several other physical problems. Following the terminology of plasma physics, we refer to this system as the single-wave model. In fact, part of the purpose of the present work was to emphasize how the single-wave model is a universal description of a transition to instability of this kind (a bifurcation of an unstable mode from a continuous spectrum). Despite this significance of the single-wave model, the system has received relatively little attention in the past. Furthermore, aside from a limited number of studies in plasma physics (see Crawford 1995), there have been no attempts to verify in detail the 'trapping scaling' on which the derivation of the model rests (that is, to solve the governing equations in the parameter regime of interest and compare with the dynamics predicted by the single-wave model). Here, we have rectified these deficiencies: we have given a broad summary of the dynamics captured by the model, ranging from the linear theory to the fully nonlinear evolution, and we have observed the trapping scaling directly in simulations of the two-dimensional fluid equations.

It is important to appreciate that trapping scaling predicts saturation levels which are significantly smaller than one might expect based on standard bifurcation analysis. One advantage of using the single-wave model is that it directly takes into account this abnormally low saturation level. Furthermore, by focusing attention on the critical layers, the model optimally places highest resolution in the regions where it is needed.

A notable feature of the dynamics predicted by the single-wave model is that at the onset of instability, provided the dissipation is sufficiently small, the mode amplitude appears to have temporally complex, perhaps chaotic, dynamics. This arises as a result of 'amplitude bounces' (trapping oscillations) that can be attributed to the sporadic creation and subsidence of secondary vortical structures within the cat's eyes. However, with limited computational resources, it is not possible to know

whether this dynamics is persistent, or merely decays slowly with time; we have given evidence to suggest that solutions are aperiodic, but the issue remains open.

If complex dynamics does persist, then the system provides an example in which chaos appears immediately beyond the onset of instability. This contrasts with many other, more familiar systems (like Rayleigh–Bénard convection) in which a sequence of bifurcations is necessary before chaos ensues. At the heart of this feature of the transition is the absence of significant dissipation. Indeed, once dissipation effectively acts within the critical layer, the vorticity begins to spread and the mode amplitude diverges, eventually breaking the trapping scaling.

The existence of temporal complexity is also relevant to Lagrangian transport theories, which have recently acquired prominence in view of various geophysical applications. In order to develop analytically, those theories often assume an equilibrated state in which the streamfunction is steady, and then artificially add a time-periodic perturbation in order to break open the steady separatrices of the cat's eye and allow transport across the jet (Samelson 1992; del Castillo-Negrete & Morrison 1993). As we see here, the unstable jet does not saturate in a steady meander, but the amplitude fluctuates. This leads to the aperiodic opening of the separatrices bounding the cat's eyes and so transport occurs naturally without the addition of other waves or perturbations. In this situation, the degree of transport can be estimated using the ideas of lobe dynamics (Rogerson *et al.* 1999). Moreover, because of its universality, the single-wave model provides a setting in which these issues can be explored in some generality (see also del Castillo-Negrete 2000).

Finally, we remark on the physical realizability of the single-wave model. A key ingredient of the model is spatial periodicity; that is, the presence of a single wave. This periodicity may be realizable in the circular geometries of experiments with electrolyte solutions (Dolzhanskii *et al.* 1991), rotating annuli (Früh & Read 1999; van de Konijnenberg *et al.* 1999; Solomon *et al.* 1993) or electron plasma columns (Driscoll & Fine 1990). But in most other physical systems one cannot quantize the system to eliminate a broad band of excited wavenumbers, as underlies the analysis here. Instead, one must include more wavenumbers, and, in particular, the effect of long spatial variations. This allows subharmonic instabilities, which lead to the pairing and merging of neighbouring vortices (Flierl *et al.* 1987). One possible way to extending the theory is to focus on long-wave instabilities, where the structure of the cat's eye and the envelope of the mode amplitude vary on a comparable spatial scale (Balmforth & Young 1997). However, secondary instabilities with short wavelength may also become important as in Rossby-wave critical layers (Haynes 1989).

We thank P. J. Morrison for helpful discussions, and M. Umurhan for help in preparing the manuscript. N. J. B. acknowledges an equipment grant from the Nuffield Foundation and a Faculty Research Grant from UCSC.

Appendix A. Numerical details

A.1. *Vorticity equation*

We solve the full two-dimensional vorticity equation using a pseudospectral scheme (kindly provided by A. Provenzale) in which we retain N Fourier components in y and $N/3$ in x. The periodic domain has size $-L \leqslant y \leqslant L$ and $-L/3 \leqslant x \leqslant L/3$, where $L \approx 5$ and is varied to control the minimum wavenumber. The flow is initialized with

the vorticity field

$$\omega(x, y, 0) = \frac{\mathrm{d}U}{\mathrm{d}y} + A_0 \operatorname{sech}^2 y(4 - k^2 - 6\operatorname{sech}^2 y) \sin kx, \tag{A 1}$$

where $U(y) = (1 + \varepsilon y)\operatorname{sech}^2 y$, and the initial perturbation amplitude was set to $A_0 = 2 \times 10^{-4}$. This approximates a jet with a superposed, low-amplitude, unstable mode.

The dissipation in the scheme arises from two sources. First, a dissipative term of the form $\nu\nabla^2\omega$ is explicitly added to the equation. This dissipative term is responsible for removing much of the power in the higher x-wavenumbers. We performed several computational test runs with a variety of values for ν in order to ensure that the results are not especially sensitive to this term. We find that a value of $\nu = 5 \times 10^{-6}$ is a convenient choice for $N = 256$ or 512. Second, there is a filter that prevents power from accumulating at higher wavenumbers. This provides a second form of dissipation that is chiefly responsible for cutting off the y-wavenumber spectrum over intermediate wavenumbers in x. The source of power in this wavenumber range comes from the action of shear tilting which cascades energy to smaller scales in y. Though the filtering is somewhat artificial we expect typical contributions of these wavenumbers to the overall dynamics to decay algebraically in time. We have also run the code at different resolutions to gauge the importance of the filter; at the parameter values we choose, the filter has a noticeable effect but the results are not overly sensitive to the position of the filter. Hence, we do not view the artifical truncation of the Fourier spectrum as being particularly serious.

A.2. *Single-wave model*

The single-wave model is solved as a partial differential equation by an operator splitting scheme described by Cheng & Knorr (1976). We first rewrite the vorticity equation in the form

$$q_T + Y q_x + \varphi_x q_Y = \lambda(q_{YY} + \kappa), \tag{A 2}$$

where $q = \zeta + \kappa\varphi - \gamma Y - \kappa Y^2/2$, and then split the integration of the equation into three stages (two advection steps and a diffusion step; see Cheng & Knorr). The integration begins from the initial condition, $q(x, Y, 0) = 2\kappa A(0)\cos x - \gamma Y - \kappa Y^2/2$, with $A(0) = 10^{-3}$. We use a variety of grid sizes: for the longer runs, we use 128 or 256 points in x and 1025 or 2049 points in Y, with a domain size of 30 for the cases at larger κ and 40 for smaller κ. Less resolution was used for the shorter runs. A maximum timestep of 2.5×10^{-5} was used. Some other details are given by Balmforth *et al.* (2000).

Although the code runs stably when $\lambda = 0$, due to the generation of ever finer scales in Y, the scheme ultimately breaks down because of its finite resolution. Thereafter, the code runs with an artificial dissipation that is difficult to both quantify and control. A comparison of runs with $\kappa = 0$ and different values for λ suggests that, for a resolution in Y of 1024 in a domain of size 30–40, the scheme has an effective viscous coefficient of 10^{-4}. For $\kappa = 1/4$, the effective dissipation was somewhat less.

We also solve the single-wave model using a particle scheme, which has some analogy to computing the characteristics of the partial differential equation. The particle orbits are constructed using the equations of motion

$$\dot{x}_n = Y_n, \quad \dot{Y}_n = \mathrm{i}(A\mathrm{e}^{\mathrm{i}x_n} - A^*\mathrm{e}^{-\mathrm{i}x_n}) \tag{A 3}$$

and

$$\mathrm{i}\dot{A} = \frac{2L}{N}\sum_{n=1}^{N}[Z_n(0) - Z_n(T)]\mathrm{e}^{-\mathrm{i}x_n}, \quad n = 1, 2, \ldots, N, \tag{A 4}$$

where N denotes the total number of particles, L is the size of the domain in Y (typically 50 or 100) and $Z_n(T) = \kappa(A\mathrm{e}^{\mathrm{i}x_n} + A^*\mathrm{e}^{-\mathrm{i}x_n}) - Y_n - \kappa Y_n^2/2$. The initial condition is composed by placing particles on a uniform grid covering the domain $-L \leqslant Y \leqslant L$ and $0 \leqslant x \leqslant 2\pi$. If $\kappa = 0$ we further exploit the symmetry of the solution to consider only the particles with $Y_n(T = 0) > 0$. The equations of motion are solved using the symplectic scheme described by Cary & Doxas (1993).

Appendix B. Derivation of the amplitude equation

With the change of frame and rescalings given in § 4.1, the governing equations become

$$\epsilon\omega_T + (S^2 - c_* + \epsilon f)\omega_x + J(\psi, \omega) = \epsilon^3\nu_3(\omega_{xx} + \omega_{yy}) + (4S^2 - 6S^4 - \beta_* - \epsilon\beta_1)\psi_x + \epsilon f_{yy}\psi_x \tag{B 1}$$

and

$$\omega = \psi_{xx} + \psi_{yy}, \tag{B 2}$$

where $S(y) = \operatorname{sech} y$.

B.1. *Regular expansion*

We begin with a regular perturbation expansion and introduce the asymptotic sequences (4.3) into (B 1), (B 2). At order ϵ^2, we find the inviscid linear equations; by our choice of basic state, the solution is the inflectional mode:

$$\psi_2 = S^2A(T)\mathrm{e}^{\mathrm{i}kx} + \text{c.c.}, \quad \omega_2 = (4 - 6S^2 - k^2)S^2[A(T)\mathrm{e}^{\mathrm{i}kx} + \text{c.c.}]. \tag{B 3}$$

In the present frame of reference, the mode is approximately stationary and develops slowly. The dependence of the solution on the long time scale, T, is yet to be determined.

At the next order, we find

$$\psi_{3yy} - 2(2 - 3S^2)\psi_3 = \left\{\left[\frac{(f_{yy} - \beta_1) - f(4 - 6S^2 - k^2)}{S^2 - c_*}\right]AS^2\mathrm{e}^{\mathrm{i}kx} - \frac{(4 - 6S^2 - k^2)}{\mathrm{i}k(S^2 - c_*)}A_TS^2\mathrm{e}^{\mathrm{i}kx} + \text{c.c.}\right\}. \tag{B 4}$$

This inhomogeneous equation will not in general have a bounded solution unless we enforce a solvability condition, obtained on multiplying by $\mathrm{e}^{-\mathrm{i}kx}S^2$ and integrating over the domain. Normally, this procedure immediately provides the evolution equation for $A(T)$. However, for the current problem, there are difficulties associated with the two critical levels because, near $y = \pm y_*$,

$$\omega_3 \sim \frac{1}{y - y_*}, \quad \psi_{3y} \sim \log(y - y_*). \tag{B 5}$$

Thus we cannot apply the solvability condition.

The divergence of the vorticity near the critical levels represents a breakdown of the asymptotic expansion. In particular, since $\omega_2 \sim 1$ as $y \to \pm y_*$, the asymptotic sequences become disordered for $y \mp y_* \sim O(\epsilon)$. This indicates that the regular

expansion scheme breaks down in thin layers surrounding each critical level. These are the modal critical layers. Here, we must rescale the cross-stream coordinate in order to resolve the layers and search for a different asymptotic solution. These inner layers are treated in the next subsection, but first we formulate the solvability condition taking them into account: we multiply (B 4) by $e^{-ikx}S^2$ and integrate over the domain, omitting the small regions $[-y_* - \delta, -y_* + \delta]$ and $[y_* - \delta, y_* + \delta]$, with $\delta \ll 1$, surrounding each critical level. Then various integrations by parts lead to

$$S_*^2[\hat{\psi}_{3y}]_{-y_*-\delta}^{-y_*+\delta} + S_*^2[\hat{\psi}_{3y}]_{y_*-\delta}^{y_*+\delta} = \frac{1}{ik} I_1 A_T + \beta_1 I_2 A, \tag{B 6}$$

where the hat represents the projection onto the Fourier mode $\exp ikx$,

$$I_1 = 4(1 - 3c_*)I_2 - 8 \tag{B 7}$$

and

$$I_2 = 2 + \frac{c_*}{\sqrt{1-c_*}} \log\left(\frac{1+\sqrt{1-c_*}}{1-\sqrt{1-c_*}}\right) \equiv 2 + \frac{c_*}{\sqrt{1-c_*}} \log K(c_*). \tag{B 8}$$

Equation (B 6) is almost the solvability condition we need to determine $A(T)$. The complication is that it explicitly contains the limits of $\hat{\psi}_{3y}$ as we enter the critical layers, and these must be determined by matching to the inner solution.

B.2. *Inner solution*

We first concentrate on the critical layer surrounding $y = y_*$. Here we introduce $y = y_* + \epsilon Y$ and the sequences,

$$\omega = \epsilon^2 Z + \cdots \tag{B 9}$$

$$\psi = \epsilon^2 \Psi_2 + \epsilon^3 \Psi_3 + \epsilon^4 \log\epsilon\, \Phi_4 + \epsilon^4 \Psi_4 + \cdots. \tag{B 10}$$

The logarithmic terms in the expansion are standard and are needed to match certain logarithmic terms appearing the outer solutions as $y \to \pm y_*$; see (B 5).

To the leading orders, the Poisson relation (2.3), becomes

$$\Psi_{2YY} = \Psi_{3YY} = \Phi_{4YY} = 0, \quad \Psi_{4YY} = Z - \Psi_{2xx}. \tag{B 11}$$

We write solutions for Ψ_2 and Ψ_3 that immediately match the leading-order inner limit of the outer stream function:

$$\Psi_2 = S_*^2(Ae^{ikx} + \text{c.c.}), \quad \Psi_3 = Y U_*'(Ae^{ikx} + \text{c.c.}), \tag{B 12}$$

where the subscript $*$ indicates the value at $y = y_*$. A similar relation can be written down for Φ_4; this function is independent of Y. Lastly,

$$[\Psi_{4Y}]_{-\Delta}^{\Delta} = \int_{-\Delta}^{\Delta} Z(x, Y, T)\, dY - 2\Delta \Psi_{2xx}. \tag{B 13}$$

When we insert the inner sequences into the vorticity equation (B 1) we find, to lowest order,

$$Z_T + (U_*'Y + f_*)Z_x + \Psi_{2x}Z_Y = \nu_3 Z_{YY} + (U_*'''Y - \beta_1 + f_*'')\Psi_{2x}. \tag{B 14}$$

Provided Z remains bounded as $Y \to \pm\infty$, we may write the far-field form: $Z U_*' \sim U_*''' \Psi_2$. It is convenient to subtract this constant far-field vorticity off the inner vorticity variable and introduce a new, localized vorticity variable,

$$\zeta_+(x, Y, T) = Z - \frac{U_*'''}{U_*'} \Psi_2. \tag{B 15}$$

The + indicates that this variable belongs to the critical layer at $y = +y_*$. Then,

$$\partial_T\zeta_+ + f_*\partial_x\zeta_+ + U_*'Y\,\partial_x\zeta_+ + \Psi_{2x}\partial_Y\zeta_+ = \nu_3\partial_Y^2\zeta_+ - \frac{U_*'''}{U_*'}\Psi_{2T} - \left(\beta_1 - f_*'' + f_*\frac{U_*'''}{U_*'}\right)\Psi_{2x}. \tag{B 16}$$

Also,

$$[\partial_Y\Psi_4^{(+)}]_{-\Delta}^{\Delta} = \int_{-\Delta}^{\Delta}\zeta_+(x,Y,T)\,\mathrm{d}Y + 2\Delta\left(\frac{U_*'''}{U_*'} + k^2\right)\Psi_2, \tag{B 17}$$

and we have added a + superscript to Ψ_4 to remind ourselves of its origin.

In an entirely analogous manner, for $y = -y_* - \epsilon Y$ and $\omega \sim \epsilon^2(U_*''\Psi_2/U_*' - \zeta_-)$, we may write equations for the second critical layer:

$$\partial_T\zeta_- - f_*\partial_x\zeta_- + U_*'Y\,\partial_x\zeta_- - \Psi_{2x}\partial_Y\zeta_- = \nu_3\partial_Y^2\zeta_- + \frac{U_*'''}{U_*'}\Psi_{2T} + \left(\beta_1 + f_*'' - f_*\frac{U_*'''}{U_*'}\right)\Psi_{2x} \tag{B 18}$$

and

$$[\partial_Y\Psi_4^{(-)}]_{-\Delta}^{\Delta} = -\int_{-\Delta}^{\Delta}\zeta_-(x,Y,T)\,\mathrm{d}Y + 2\Delta\left(\frac{U_*'''}{U_*'} + k^2\right)\Psi_2, \tag{B 19}$$

where we have exploited the symmetries of S^2 and $f(y)$. It is convenient to introduce a shift of the x-coordinate in these equations: $x \to x + \pi/k$. Then $\Psi_2 \to -\Psi_2$, and the vorticity equation is put in the form

$$\partial_T\zeta_- - f_*\partial_x\zeta_- + U_*'Y\,\partial_x\zeta_- + \Psi_{2x}\partial_Y\zeta_- = \nu_3\partial_Y^2\zeta_- - \frac{U_*'''}{U_*'}\Psi_{2T} - \left(\beta_1 + f_*'' - f_*\frac{U_*'''}{U_*'}\right)\Psi_{2x}, \tag{B 20}$$

which differs from (B 16) only by the terms involving the asymmetrical perturbation, f.

B.3. *Matching*

Now we match the inner and outer solutions. The explicit choices of Ψ_2, Ψ_3 and Φ_4 in (B 12) ensure a match of the leading-order streamfunction. Likewise, it is not difficult to show that the far-field forms of the critical-layer vorticities match with the inner limits of the outer solution. The only part that requires some discussion is the match of the streamwise velocity, ψ_y.

To match this velocity component, we write the inner limit of the outer solution:

$$\psi_y = \pm\epsilon^2\psi_{2*y} + \epsilon^3\left[\pm\psi_{3*y} + \frac{(y \mp y_*)}{\epsilon}\psi_{2*yy}\right] + \cdots. \tag{B 21}$$

The outer limit of the inner solution, on the other hand, is

$$\Psi_y \equiv \pm\frac{1}{\epsilon}\Psi_Y = \pm\epsilon^2\Psi_{3Y} \pm \epsilon^3\Psi_{4Y}^{(\pm)} + \cdots. \tag{B 22}$$

By writing the outer coordinate y in terms of the inner coordinates Y, and defining $\Delta = \delta/\epsilon$, we may match these expressions term by term in an intermediate matching region where $\epsilon \ll \delta \ll 1$ or $1 \ll \Delta \ll \epsilon^{-1}$. The leading order is automatically satisfied, and the order-ϵ^3 terms provide the relation

$$[\psi_{3y}]_{y_*-\delta}^{y_*+\delta} + 2\Delta\psi_{2yy} = [\partial_Y\Psi_4^{(+)}]_{-\Delta}^{\Delta} = \int_{-\Delta}^{\Delta}\zeta_+\mathrm{d}Y + 2\Delta\left(\frac{U_*'''}{U_*'} + k^2\right)\Psi_2, \tag{B 23}$$

with an analogous expression for the jump across the other critical layer. On recalling

the reflection of Y and the shift of x in the $y=-y_*$ critical layer, we arrive at

$$[\psi_{3y}]_{y_*-\delta}^{y_*+\delta}+[\psi_{3y}]_{-y_*-\delta}^{-y_*+\delta}=\int_{-\Delta}^{\Delta}[\zeta_+(x,Y,T)-\zeta_-(x-\pi/k,Y,T)]\,\mathrm{d}Y. \tag{B 24}$$

Note that, by matching the jump in ψ_y, we can avoid a discussion of the logarithmic terms that formally complicate the expansion. However, we must interpret the final relation in terms of principal values because ψ_{3y} and the integral diverge logarithmically in the relevant limits.

This expression is needed in our solvability condition, which we now write as

$$\frac{1}{\mathrm{i}k}I_1A_T+\beta_1I_2A=\frac{kS_*^2}{2\pi}\int_{-\infty}^{\infty}\int_0^{2\pi/k}\mathrm{e}^{-\mathrm{i}kx}[\zeta_+(x,Y,T)+\zeta_-(x,Y,T)]\,\mathrm{d}x\mathrm{d}Y, \tag{B 25}$$

on letting $\Delta\to\infty$.

B.4. *Canonical form*

We place the equations governing the mode dynamics into a canonical form by introducing some rescalings and new parameters:

$$x'=kx-k\beta_1\frac{I_2}{I_1}T,\quad Y'=\frac{Y-Y_{0\pm}}{\alpha},\quad T'=\frac{T}{\tau},\quad A'=\frac{A}{a}\mathrm{e}^{\mathrm{i}k\beta_1I_2T/I_1}, \tag{B 26}$$

$$\varphi=\frac{\Psi_2}{ac_*},\quad \zeta'_\pm=\frac{\zeta_\pm}{b},\quad \lambda=\frac{\nu_3\tau}{\alpha^2},\quad \kappa=2c_*^2\frac{U'''_*}{I_1(U'_*)^2}, \tag{B 27}$$

$$\gamma=\frac{a\tau}{b}c_*k\beta_1\left[1-\frac{I_2U'''_*}{I_1U'_*}\right],\quad \sigma=\frac{a\tau}{b}c_*k\left(f''_*-f_*\frac{U'''_*}{U'_*}\right), \tag{B 28}$$

where

$$\alpha=\frac{1}{kU'_*\tau},\quad a=\frac{1}{k^2c_*U'_*\tau^2},\quad b=\frac{I_1}{2k^2c_*^2\tau^2},\quad Y_{0\pm}=\frac{1}{U'_*}\left[\frac{\beta_1I_2}{I_1}\mp f_*\right]. \tag{B 29}$$

The final relations provide choices for three of the four scaling variables, a, b, α and τ; we have written the formulae with τ undefined. We may use that fourth variable to scale one of γ, κ or σ to unity in absolute value (provided that parameter is non-zero). For the numerical computations reported in the main text, we exploit this scaling to set $\gamma=-1$.

On dropping the primes, we find the equations quoted in § 4.1.

Appendix C. Asymptotic limits

The single-wave model has the two parameters, λ and κ. In the special limits in which one of these parameters becomes large, the model can be reduced to simpler forms.

C.1. $\lambda\gg1$

For $\lambda\gg1$, the evolution is dominated by the viscosity. In this situation, the vorticity diffuses rapidly throughout the critical region, resulting in a relatively wide cat's eye pattern and a strong mode amplitude. This is captured in the rescalings

$$Y=\lambda^{1/3}\tilde{Y},\quad A=\lambda^{2/3}\tilde{A},\quad \zeta=\lambda^{1/3}\tilde{\zeta}. \tag{C 1}$$

In terms of the new variables, the system becomes

$$\lambda^{-1/3}\tilde{\zeta}_T + \tilde{Y}\,\tilde{\zeta}_x + \tilde{\varphi}_x\tilde{\zeta}_{\tilde{Y}} = \tilde{\zeta}_{\tilde{Y}\tilde{Y}} - \gamma\tilde{\varphi}_x - \kappa\tilde{\varphi}_T, \tag{C 2}$$

$$\mathrm{i}\tilde{A}_T = \langle \mathrm{e}^{-\mathrm{i}x}\tilde{\zeta}\rangle, \quad \tilde{\varphi} = \tilde{A}\mathrm{e}^{-\mathrm{i}x} + \text{c.c.} \tag{C 3}$$

Thus, to leading order, the time derivative drops out of the vorticity equation and the vorticity distribution evolves quasi-statically, which is permitted because of the relatively strong dissipation.

C.2. $\kappa \gg 1$, $\lambda \neq 0$

For large κ, a similar simplification occurs. To see this, we first transform into a moving frame by writing

$$x = X + \frac{\gamma}{\kappa}T, \quad \partial_T \to \partial_T - \frac{\gamma}{\kappa}\partial_x, \quad A = \hat{A}\mathrm{e}^{\mathrm{i}\gamma T/\kappa}, \tag{C 4}$$

and then set $\tau = T/\kappa^2$ and $\zeta = \kappa^{-1}\hat{\zeta}$. Thence,

$$\kappa^{-2}\hat{\zeta}_\tau - \kappa^{-1}\gamma\hat{\zeta}_X + Y\,\hat{\zeta}_X + \varphi_X\tilde{\zeta}_Y = \lambda\hat{\zeta}_{YY} - \tilde{\varphi}_\tau, \tag{C 5}$$

$$-\gamma\hat{A} + \mathrm{i}\kappa^{-1}\hat{A}_T = \langle \mathrm{e}^{-\mathrm{i}X}\tilde{\zeta}\rangle, \quad \tilde{\varphi} = \hat{A}\mathrm{e}^{-\mathrm{i}X} + \text{c.c.} \tag{C 6}$$

To leading order, we once again find a quasi-steady critical layer. We also lose the time derivative from the A-equation but this is not essential to the approximation (the term, $\tilde{\varphi}_\tau$, remains on the right-hand of the vorticity equation). The key effect here is that a strong κ slows down the evolution of the mode so much as to allow viscosity to equilibrate the critical layer. Thus we once again enter the regime of large dissipation.

C.3. *Quasi-steady critical layers*

We can capture both limits above by simply dropping the time derivative from the vorticity equation. Then, in the original variables,

$$Y\,\zeta_x + \varphi_x\zeta_Y = \lambda\zeta_{YY} - \gamma\varphi_x - \kappa\varphi_T, \tag{C 7}$$

$$\mathrm{i}A_T = \langle \mathrm{e}^{-\mathrm{i}x}\zeta\rangle, \quad \varphi = A\mathrm{e}^{-\mathrm{i}x} + \text{c.c.} \tag{C 8}$$

Next, let $A = -a\mathrm{e}^{\mathrm{i}\Theta}$, $g = \zeta$, $\xi = x + \Theta$ and $Y = \eta\sqrt{2a}$. Then,

$$\eta g_\xi + g_\eta \sin\xi - \hat{\lambda}g_{\eta\eta} = [(\gamma + \kappa\Theta_T)a\sin\xi - \kappa a_T\cos\xi]\sqrt{2/a}, \tag{C 9}$$

$$a\Theta_T = -\sqrt{2a}\langle\zeta\cos\xi\rangle_{\xi,\eta}, \quad a_T = -\sqrt{2a}\langle\zeta\sin\xi\rangle_{\xi,\eta}, \tag{C 10}$$

where $\hat{\lambda} = \lambda/(2a)^{3/2}$. Thus,

$$g = [-(\gamma + \kappa\Theta_T)ag_1(\xi,\eta;\hat{\lambda}) + \kappa a_T g_2(\xi,\eta;\hat{\lambda})]\sqrt{1/2a}, \tag{C 11}$$

where $g_1(\xi,\eta;\hat{\lambda})$ and $g_2(\xi,\eta;\hat{\lambda})$ are functions defined by Churilov & Shukhman (1996) that satisfy

$$\eta g_{1\xi} + g_{1\eta}\sin\xi - \hat{\lambda}g_{1\eta\eta} = -2\sin\xi, \quad \eta g_{2\xi} + g_{2\eta}\sin\xi - \hat{\lambda}g_{2\eta\eta} = -2\cos\xi. \tag{C 12}$$

Furthermore, in their notation,

$$\langle g_1\sin\xi\rangle_{\xi,\eta} = \Phi_1(\hat{\lambda}), \quad \langle g_1\cos\xi\rangle_{\xi,\eta} = 0, \quad \langle g_2\sin\xi\rangle_{\xi,\eta} = 0, \quad \langle g_2\cos\xi\rangle_{\xi,\eta} = \Phi_2(\hat{\lambda}), \tag{C 13}$$

in which $\Phi_1(\hat{\lambda})$ and $\Phi_2(\hat{\lambda})$ are known (computed) functions. Therefore,

$$a\Theta_T = -\kappa a_T \Phi_2[\lambda/(2a)^{3/2}], \quad a_T = (\gamma + \kappa\Theta_T)a\Phi_1[\lambda/(2a)^{3/2}], \tag{C 14}$$

which can be rearranged into a first-order ordinary differential equation. These equations are of finite dimension and predict that $a \sim t^{2/3}$ for unstable systems at large times. Both features result from the relatively large viscosity, which breaks the inviscid character of the system, and causes the critical layer to spread.

REFERENCES

Balmforth, N. J. 1998 Stability of vorticity defects in viscous shear. *J. Fluid Mech.* **357**, 199–224.

Balmforth N. J. 1999 Shear instability in shallow water. *J. Fluid Mech.* **387**, 97–127.

Balmforth, N. J., Llewellyn Smith, S. G. & Young, W. R. 2000 Disturbing vortices. *J. Fluid Mech.* **426**, 95–133.

Balmforth, N. J. & Young, W. R. 1997 Longwave instability in shear flows. *Phys. Rev. Lett.* **79**, 4155–4159.

Brown, S. N. & Stewartson, K. 1978 The evolution of the critical layer of a Rossby wave. Part II. *Geophys. Astrophys. Fluid Dyn.* **10**, 1–24.

Cary, J. R. & Doxas, I. 1993 An explicit symplectic integration scheme for plasma simulations. *J. Comp. Phys.* **107**, 98–104.

del Castillo-Negrete, D. 1998 Weakly nonlinear dynamics of electrostatic perturbations in marginally stable plasmas. *Phys. Plasmas* **5**, 3886–3900.

del Castillo-Negrete, D. 2000 Self-consistent transport in fluids and plasmas. *Chaos* **10**, 75–88.

del Castillo-Negrete, D. & Morrison, P. J. 1993 Chaotic advection by Rossby waves in shear flow. *Phys. Fluids* A **5**, 948–965.

Cheng, C. Z. & Knorr, G. 1976 The integration of the Vlasov equation in configuration space. *J. Comput. Phys.* **22**, 330–351.

Churilov, S. M. & Shukhman, I. G. 1987 The nonlinear development of disturbances in a zonal shear flow. *Geophys. Astrophys. Fluid Dyn.* **38**, 145–175.

Churilov, S. M. & Shukhman, I. G. 1996 The nonlinear critical layer resulting from the spatial or temporal evolution of weakly unstable disturbances in shear flows. *J. Fluid Mech.* **318**, 189–221.

Crawford, J. D. 1995 Amplitude equations for electrostatic waves: universal behaviour in the limit of weak instability. *Phys. Plasmas* **2**, 97–128.

Dolzhanskii, F. V., Krymov, V. A. & Manin, D. Y. 1991 Stability and vortex structures of quasi-two-dimensional shear flow. *Sov. Phys. Usp.* **33**, 495.

Drazin, P. G., Beaumont, D. N. & Coaker, S. A. 1982 On Rossby waves modified by basic shear, and barotropic instability. *J. Fluid Mech.* **124**, 439–456.

Driscoll, C. F. & Fine, K. S. 1990 Experiments on vortex dynamics in pure electron plasma. *Phys. Fluids* B **2**, 1359–1366.

Flierl, G. R., Malanotte-Rizzoli, P. & Zabusky, N. J. 1987 Nonlinear waves and coherent vortex structures in barotropic β-plane jets. *J. Phys. Oceanogr.* **17**, 1408–1438.

Früh, W.-G. & Read, P. L. 1999 Experiments on a barotropic rotating shear layer. Part 1. Instability and steady vortices. *J. Fluid Mech.* **383**, 143–173.

Goldstein, M. E. & Hultgren, L. S. 1988 Nonlinear spatial evolution of an externally excited instability wave in a free shear layer. *J. Fluid Mech.* **197**, 259–330.

Goldstein, M. E. & Leib, S. J. 1988 Nonlinear roll-up of externally excited free shear layers. *J. Fluid Mech.* **191**, 481–515.

Haynes, P. H. 1989 The effect of barotropic instability on the nonlinear evolution of a Rossby-wave critical layer. *J. Fluid Mech.* **207**, 231–266.

Howard, L. N. 1964 The number of unstable modes in hydrodynamic stability problems. *J. Méc.* **3**, 433–443.

Howard, L. N. & Drazin, P. G. 1964 On instability of parallel flow of inviscid fluid in a rotating system with variable coriolis parameter. *J. Math. Phys.* **43**, 83–99.

van de Konijnenberg, J. A., Nielsen, A. H., Rasmussen, J. J. & Stenum, B. 1999 Shear flow instability in a rotating fluid. *J. Fluid Mech.* **387**, 177–204.

Kwon, H. J. & Mak, M. 1988 On the equilibration in nonlinear barotropic instability. *J. Atmos. Sci.* **45**, 294–308.

Leib, S. J. & Goldstein, M. E. 1989 Nonlinear interaction between the sinuous and varicose instability modes in a plane wake. *Phys. Fluids* A **1**, 513–521.

Lipps, F. B. 1962 The barotropic stability of the mean winds in the atmosphere. *J. Fluid Mech.* **12**, 397–407.

Manfredi, G. 1997 Long-time behaviour of nonlinear Landau damping. *Phys. Rev. Lett.* **79**, 2815–2819.

Maslowe, S. A. 1991 Barotropic instability of the Bickley jet. *J. Fluid Mech.* **229**, 417–426.

Miura, A. & Sato, T. 1978 Theory of vortex nutation and amplitude oscillation in an inviscid shear instability. *J. Fluid Mech.* **86**, 33–47.

O'Neil, T. M. 1965 Collisionless damping of nonlinear plasma oscillations. *Phys. Fluids* **8**, 2255–2262.

O'Neil, T. M., Winfrey, J. H. & Malmberg, J. H. 1971 Nonlinear interaction of a small cold beam and a plasma. *Phys. Fluids* **14**, 1204–1212.

Onishchenko, I. N., Linetskii, A. R., Matsiborko, N. G., Shapiro, V. D. & Shevchenko, V. I. 1971 On nonlinear theory of instability of a monoenergetic electron beam. *Sov. Phys. JETP* **11**, 281–285.

Rogerson, A. M., Miller, P. D., Pratt, L. J. & Jones, C. K. R. T. 1999 Lagrangian motion and fluid exchange in a barotropic meandering jet. *J. Phys. Oceanogr.* **29**, 2635–2655.

Samelson, R. M. 1992 Fluid exchange across a meandering jet. *J. Phys. Oceanogr.* **22**, 431–440.

Solomon, T. H., Holloway, W. J. & Swinney, H. 1993 Shear flow instabilities and Rossby waves in barotropic fluid in a rotating annulus. *Phys. Fluids* A **5**, 1971–1988.

Stewartson, K. 1978 The evolution of the critical layer of a Rossby wave. *Geophys. Astrophys. Fluid Dyn.* **9**, 185–200.

Tennyson, J. L., Meiss, J. D. & Morrison, P. J. 1994 Self-consistent chaos in the beam-plasma instability. *Physica* D **71**, 1–17.